Nanoscale

ROYAL SOCIETY OF CHEMISTRY

REVIEW

View Article Online
View Journal | View Issue

Cite this: *Nanoscale*, 2020, **12**, 20065

Molecular gold strings: aurophilicity, luminescence and structure–property correlations

Tim P. Seifert, Vanitha R. Naina, Thomas J. Feuerstein, Nicolai D. Knöfel and Peter W. Roesky *

This review covers the compound class of one-dimensional gold strings. These compounds feature a formally infinite repetition of gold complexes as monomers/repeating units that are held together by aurophilic interactions, *i.e.* direct gold–gold contacts. Their molecular structures are primarily determined in the solid state using single crystal X-ray diffraction. The chemical composition of the employed gold complexes is diverse and furthermore plays a key role in terms of structure characteristics and the resulting properties. One of the most common features of gold strings is their photoluminescence upon UV excitation. The emission energy is often dependent on the distance of adjacent gold ions and the electronic structure of the whole string. In terms of gold strings, these parameters can be fine-tuned by external stimuli such as solvent, pH value, pressure or mechanical stress. This leads to direct structure–property correlations, not only with regard to the photophysical properties, but also electric conductivity for potential application in nanoelectronics. Concerning these correlations, gold strings, consisting of self-assembled individual complexes as building blocks, are the ideal compound class to look at, as perturbations by an inhomogeneity in the ligand sphere (such as the end of a molecule) can be neglected. Therefore, the aim of this review is to shed light on the past achievements and current developments in this area.

Received 23rd June 2020,
Accepted 12th August 2020

DOI: 10.1039/d0nr04748a

rsc.li/nanoscale

Institute of Inorganic Chemistry, Karlsruhe Institute of Technology (KIT), Engesserstr. 15, 76131 Karlsruhe, Germany. E-mail: roesky@kit.edu

Introduction

A. General considerations for molecular one-dimensional gold strings and their properties

In the age of nanotechnology, interest in materials with tailor-made properties is steadily increasing. Since physical properties are often dependent on the molecular structure, there is a general demand for precise and well-investigated materials.[1] One of the crucial factors is the molecular dimen-

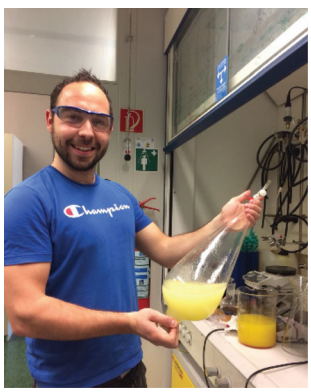

Tim P. Seifert

Tim P. Seifert received his Master's Degree in Chemistry from Karlsruhe Institute of Technology in 2015. He then joined the inorganic chemistry department in the group of Professor Peter Roesky, where he obtained his PhD degree in 2018. He is currently enrolled as a postdoctoral researcher in the same group. His research interests include metallophilic interactions in a luminescence and fundamental context.

Vanitha R. Naina

Vanitha Reddy Naina received her Master's Degree in 2019 from the Discipline of Chemistry, Indian Institute of Technology Indore, India, during which she was a recipient of the DAAD India IIT Master Sandwich Program in 2018. She is currently pursuing her doctoral research in chemistry at Karlsruhe Institute of Technology in the research group of Prof. Dr Peter W. Roesky. Her current research work is focused on luminescent metal complexes.

sionality of the material, which, in the case of properties and applications, is impressively demonstrated by the carbon modifications graphite, graphene, carbon nanotubes and fullerenes as 3D, 2D, 1D and 0D materials, respectively.[2–7] The major driving forces for research on one-dimensional substances are typically their conductive properties and potential application in nanoelectronics as molecular wires.[8] Besides the development of organic 1D conductors, organometallic complexes that exhibit a chain-like structure are in the focus of interest as well.[9–14] A defined linear arrangement of metal ions is not only a potential molecular wire, yet highly interesting from a fundamental and theoretical point of view. Examples range from epitaxial crystal growth,[15] non-linear optical behaviour[16,17] and metal-containing liquid crystals (MLC)[18] to anisotropic electrical conductivity.[19–25] Synthetic approaches towards such metal strings include ligand-enforced arrangement of metal ions, as seen in the undecametallic $[Ni_{11}(tentra)_4Cl_2](PF_6)_4$ (tentra = tetranaphthyridyltriamine) complex[26] or metallophilic interactions as design elements. In the latter, especially d^8 and d^{10} configured ions are utilized for the synthesis of one-dimensional metal strings.[27–31] In this review, focus is put on formally infinite molecular gold strings with homogeneous repeating units, because their specific properties can be assigned to defined structural features.[32] In contrast, finite (oligomeric) gold strings in small molecules have 'dead ends' or an inhomogeneous saturation of the coordination sphere caused by the respective ligand system and thus, deviations in structure–property relationships might be induced.[27,33,34] While related metal strings or metal string complexes of a series of elements have already been discussed and reviewed,[25,35–48] we think a critical update on the unique chemistry of gold strings is valuable at this point.

B. Aurophilicity and metallophilicity

When X-ray diffraction became more and more popular for the definite elucidation of molecular structures in the 1970s, some structural features of simple gold-containing compounds could not be explained anymore by the standard concepts of valence and chemical bonding. Namely, gold atoms (especially in their +I oxidation state) were observed to be in close proximity, even below the sum of their van der Waals radii, which suggested a strong attractive interaction between these cations.[49–51] This was indeed unusual, as Coulomb repulsion should evoke the opposite effect. Furthermore, Au(I) exhibits a closed-shell ($[Xe]4f^{14}5d^{10}$) electron configuration and an interaction of such systems was simply not expected. These early observations gave rise to a hitherto unknown research field. Not surprisingly, this curiosity soon became interesting from a theoretical point of view as well.[52] A major breakthrough was achieved in the early 1990s, when P. Pyykkö studied varying Au–Au distances in the model complex $[(AuCl(PH_3))_2]$ at the Hartree–Fock (HF) and second order Møller–Plesset (MP2) levels. While the HF curve showed a purely repulsive behaviour, attraction was observed at the MP2 level, which could be attributed to the dispersive part of electron-correlation effects.[53] In addition, the interaction decreases with the Au–Au separation (R) like R^{-6}, hence following the rules of the London dispersion force (LDF).[54,55] Thus, in a simple picture, these Au–Au attractions are van der Waals interactions, but unusually strong ones due to relativistic effects. To this date, this interpretation has been supported by many studies and is generally accepted,[56–61] although discussions about the concept are still on-going to this date.[62,63] At first, those interactions were believed to only emerge for gold; hence the term 'aurophilic interactions' or 'aurophilicity' was established by H. Schmidbaur in 1989 to describe the phenomenon.[64,65] In general, these terms are used commonly if the distance between two gold atoms falls below the limit of 3.5 Å, for which bonding can still be considered, although the respective van der Waals distance (3.32 Å)[66] is shorter.[67,68] Hereby, the Au–Au distance is correlated with the strength of these interactions, which can reach values of up to 50 kJ mol^{-1}, *i.e.* com-

Thomas J. Feuerstein

Thomas J. Feuerstein obtained his M.Sc. degree in Chemistry at Karlsruhe Institute of Technology (KIT) in 2015. Afterwards he joined the workgroup of Professor Peter Roesky where he obtained his PhD degree in 2019. Currently he works as a postdoctoral researcher in the same group. His research interests are photoluminescent metal compounds, especially coinage metals, and their investigation under cryogenic conditions.

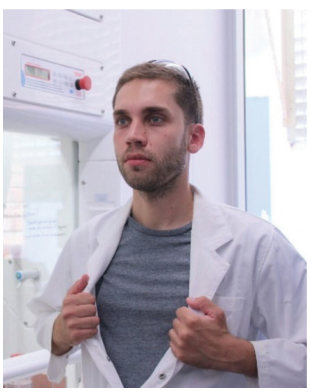

Nicolai D. Knöfel

Nicolai D. Knöfel obtained his Master's degree in Chemistry at Karlsruhe Institute of Technology (KIT) in 2015, followed by a PhD study in the workgroup of Professor Peter W. Roesky (Inorganic Chemistry department, KIT). He received his PhD degree in 2019 with distinction and proceeded as a postdoctoral researcher in the same working group for one year. His research fields comprise metallopolymers and multiply bonded transition metal complexes. Sometimes he also writes reviews.

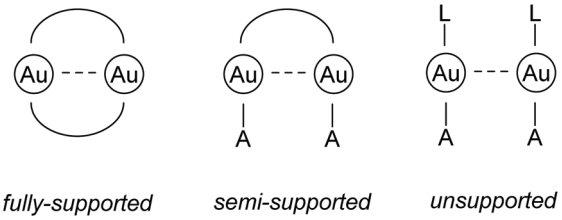

Fig. 1 Schematic drawings of different subtypes of aurophilic interactions. L = neutral donor ligand; A = anionic ligand.[68]

parable with hydrogen bonds. Based on findings by P. Schwerdtfeger, the energy can be estimated according to

$$E_{\mathrm{Au\text{–}Au}} = 1.27 \times 10^6 e^{-3.5d(\mathrm{Au\text{–}Au})} \quad (1)$$

where E is the energy in kJ mol^{-1} and d(Au–Au) is the gold–gold distance in Å.[56,57] Depending on the type of ligand, the interactions are further subdivided into fully-supported, semi-supported and unsupported interactions. Any kind of intermolecular aurophilic interaction is described as 'unsupported'. In contrast, supported interactions include a molecular framework, in which the aurophilic contact is promoted by entropic contributions, structural rigidity or a preorganized ligand scaffold (Fig. 1).[67,68]

While it is assumed that fully supported interactions are maintained in solution, the bonding situation of semi- and unsupported interactions in solution cannot be generalized and has to be evaluated in each case individually, because the solvation energy can compensate the comparably weak energy gain resulting from aurophilic interactions.[67,69–73]

Peter W. Roesky

Peter W. Roesky obtained his diploma in 1992 from the University of Würzburg and his doctoral degree from the Technical University of Munich (with Prof. W. A. Herrmann) in 1994. He was as a postdoc with Prof. T. J. Marks at Northwestern University (1995–1996). In 1999 he completed his Habilitation at the University of Karlsruhe. As a full professor he joined the faculty of the Freie Universität Berlin in 2001. Since 2008 he has held the chair for inorganic functional materials at the University of Karlsruhe Institute of Technology. In 1999 he received a Heisenberg scholarship of the German Science Foundation, and in 2000 a Karl–Winnacker scholarship. Since 2014 he is a fellow of the Royal Society of Chemistry and since 2020 a fellow of the European Academy of Science (EurAsc). In 2019 he received a JSPS Invitational Fellowship for Research in Japan and in 2020 a Reinhart Koselleck Project of the German Science Foundation.

The upcoming of aurophilicity attracted interest in similar interactions of other closed-shell ions as well. For example, R. Hoffmann and M. Jansen observed very short intermetallic distances for the lighter d^{10} configured homologues Cu(I) and Ag(I) in 1978 and 1987, respectively.[74,75] Today, numerous elements, including open-shell ions like Au(III), Pt(II), Pd(II), Ir(I) or Ru(0), are known to interact with other heavy metal ions, expanding the concept to '*metallophilic interactions*', even though pure aurophilic interactions are typically the strongest among them and therefore still take a special place.[36,39,76–83]

C. Luminescence

Among the properties of molecular 1D gold(I) chains, particular interest lies in the investigation of their photophysical characteristics.[84–86] Heavy atoms like gold enhance spin–orbit coupling of the respective system, which facilitates transitions to the triplet manifold *via* intersystem crossing (ISC). Therefore, effective phosphorescence is regularly observed, manifested by large Stokes shifts and luminescence decay times in the lower microsecond range.[87] Besides that, the emission properties can be further perturbed in the presence of aurophilic interactions. A prominent example addressing this issue was reported by Yam *et al.*,[88] in which the luminescence of gold(I) complexes is directly affected and enhanced in the presence of an alkali metal crown ether complex, resulting in the formation of short Au–Au contacts. The perturbation induces a shift towards a lower emission energy. Therefore, it was assumed that the aurophilic interaction alters the emissive ligand to metal charge transfer (LMCT) state into a ligand to metal–metal charge transfer (LMMCT) state that goes along with a smaller HOMO–LUMO gap (Fig. 2). Additionally, besides the common LMCT emissive states, MLCT (metal to ligand charge transfer) processes for Au(I) complexes are known, which

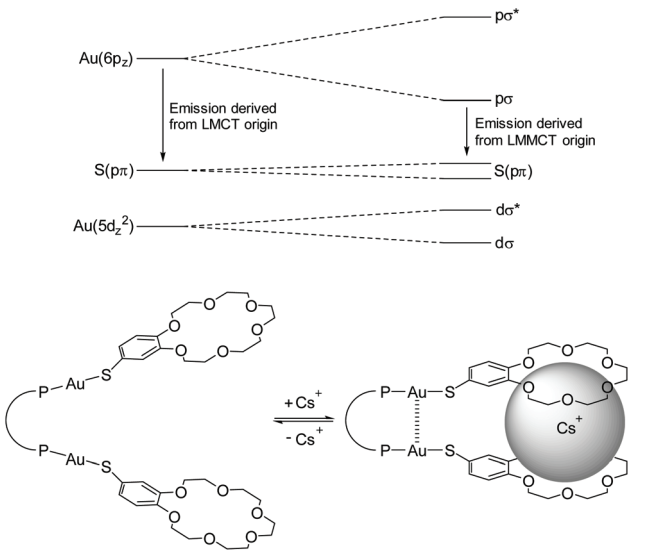

Fig. 2 Schematic representation of orbital splittings induced by to aurophilic interactions in dinuclear gold(I) thiolate complexes. Adapted with permission.[88] Copyright 2004 American Chemical Society.

is mainly due to the oxidizing as well as reducing capability of Au(I) ions. Absorptions, which can be attributed to MLCT states, are primarily observed in complexes with π-acceptor ligands like cyanides, isocyanides and phosphines.[89,90] However, these usually feature high energy absorptions and therefore, typical MLCT absorption bands are observed at comparably short wavelengths between 230 and 250 nm.[91]

It has been predicted that the alteration from LMCT towards LMMCT states further enhances when three gold(I) ions interact linearly, due to a δ combination of three instead of two $d_{x^2-y^2}$ orbitals (Fig. 3). This interesting phenomenon is particularly anticipated for 'infinite' 1D gold(I) chains.[92] Moreover, as unsupported aurophilic interactions are the main assembly motif of 1D gold chains, a perturbation *via* different environmental stimuli is readily achieved in many cases and often goes along with a significant change of the structural and photophysical properties.

From a photophysical point of view, this represents the most important aspect of the herein presented 1D structures, as diverse slight stimuli already have an impact on the rather weak aurophilic interactions. Possible stimuli include solvent, pH value, pressure, and mechanical stress as well as temperature.[84] This makes them a promising compound class towards an application as luminescent sensors and has already been remarkably demonstrated in recent reports, in which 1D gold(I) chains were found to show unique properties like solvatochromism,[94] mechanochromism[95] and luminescence tribochromism.[96] In addition, this compound class is especially valuable to gain a better understanding of metallophilic interactions in general.

D. Classification of molecular gold strings

In the crystalline state of many gold-containing complexes, a clear tendency towards the development of aurophilic interactions is observed. However, from a synthetic point of view, it is challenging to predict whether this manifests in the formation of dimers, oligomers or 'infinite' (mostly one-dimensional) self-assembled polymers.[97] Most importantly, the combination of steric and electronic demands of the respective ligand sphere plays a decisive role.[98,99] 1D gold chains are generated by an aurophilicity-induced self-assembly of molecular complexes; therefore a general distinction between ionic and neutral 'chain links' is reasonable, since the presence or absence of Coulomb interactions is an additional key factor. Hereby, ionic chains feature (mostly) homoleptic $[A\text{-}Au\text{-}A]^-$, $[L\text{-}Au\text{-}L]^+$ (A = anion; L = neutral donor) moieties or a combination of both anionic and cationic species. Due to the ionic character, these compounds often show a good solubility in polar solvents such as water. A neutral 'chain link' or complex, if Au(I) is taken as an example, consists of a monoanionic ligand paired with a neutral donor molecule coordinated to the central gold atom. Notably, heteroleptic neutral compounds often show a ligand exchange equilibrium in solution and an ionic homoleptic species is observed in the crystalline state. This is particularly valid for small and monodentate ligands like thiophene, pyridine, halogenides and pseudo-halogenides.[100–103] Therefore, the different synthetic approaches, as well as the resulting molecular structures, are differentiated by the classification presented in Fig. 4. Within the scope of this review, the different classes are shortly introduced and selected publications, highlighting extraordinary research results and major breakthroughs, are presented in detail.

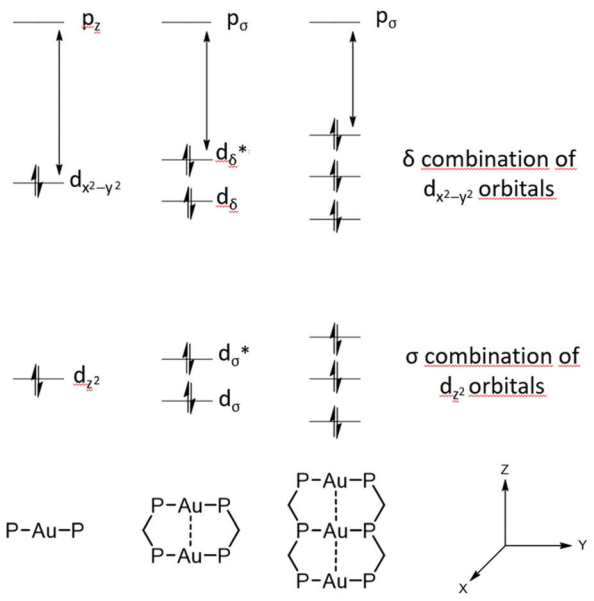

Fig. 3 Molecular-orbital interactions for stacking of d^{10} AuP_2 units in D_{2h} symmetry.[93]

Gold strings with ionic chains

Purely cationic chain links

The few examples of gold strings, in which the respective countercations or -anions are simple organic or weakly coordinating molecules, are particularly interesting, since the aurophilic attraction overcompensates the Coulomb repulsion, resulting in a sequence of 'infinite' adjacent anions or cations.[104–106]

Already in 1974, the Balch group introduced a synthetic procedure for cationic bis(carbene) gold(I) complexes by addition of isocyanides and primary amines to aqueous solutions of $[AuCl_4]^-$ salts. The reaction readily yields compounds of the type $[Au\{C(NR_2)(NR'H)\}_2]^+$.[107] Following this procedure, using methylisocyanide and methylamine, a series of symmetrically substituted bis(carbene) gold(I) complexes $[Au\{C(NHMe)_2\}_2]^+$ with varying anions (PF_6^- (**1a**), BF_4^- (**1b**), AsF_6^-, SbF_6^-) were presented in 2002 and 2008 by the same group (Scheme 1).[108–110]

As observed in the crystal structure, the PF_6^- salt **1a** consists of a linear coordinated gold(I) center with the ligands being arranged coplanarly. The cations form a linear gold chain along a crystallographic 4_2 axis comprising relatively short Au–Au contacts (3.1882(1) Å). Furthermore, the carbene ligands are linked to the PF_6 ion *via* hydrogen bonds from the NH-moieties (Fig. 5, left). For **1b** (anion = BF_4^-), the Au–Au bond lengths are elongated (d_{Au-Au} = 3.4615(2) Å), while the

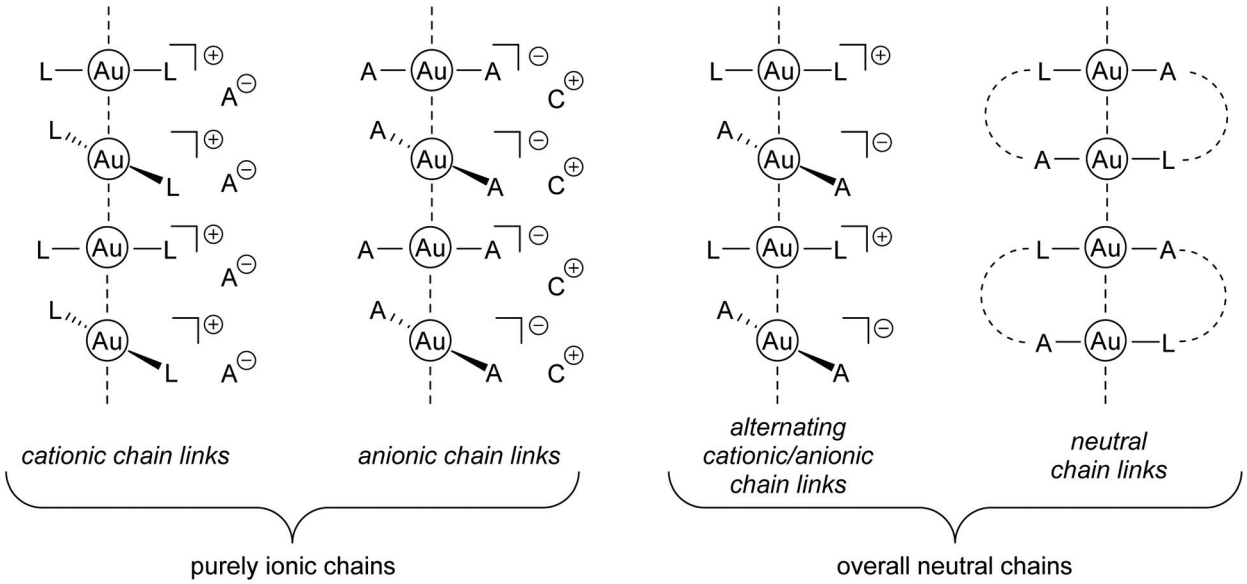

Fig. 4 Schematic drawing of gold strings consisting of Au(I) chain links with neutral or ionic building blocks (A = anion, C = cation, L = neutral ligand).

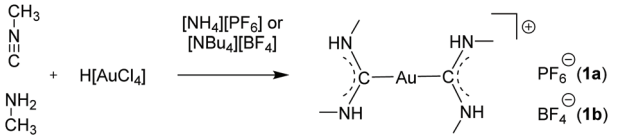

Scheme 1 Synthesis of bis(carbene) gold complexes **1a** and **1b**.

angles are in a comparable range to **1a** ($angle_{C–Au–C}$ = 178.42 (12)°). In addition, the relative ligand orientation differs in a way that the outer methyl groups face one another. The same applies for the N–H groups, which allow the formation of hydrogen bonds from one cation to two different fluorine atoms of the BF_4 ion (Fig. 5, right). Both **1a** and **1b** are colourless solids and display photoluminescence behaviour. Exemplarily, **1a** shows green-blue (λ_{max} = 460 nm) luminescence upon UV irradiation at 300 K. Upon cooling to 77 K, two emission bands are observed, whereby the maximum of the more intense emission is significantly red shifted. When dissolved in solvents like acetone, pyridine, dimethylsulfoxide (DMSO), dimethylformamide (DMF) or acetonitrile, the resulting colourless solutions are not luminescent anymore. However, upon freezing in liquid N_2, the solutions become intensely luminescent again and strikingly, the emission colours differ in varying solvents (Fig. 6). This process is entirely reversible as the thawed solutions lose their photo-

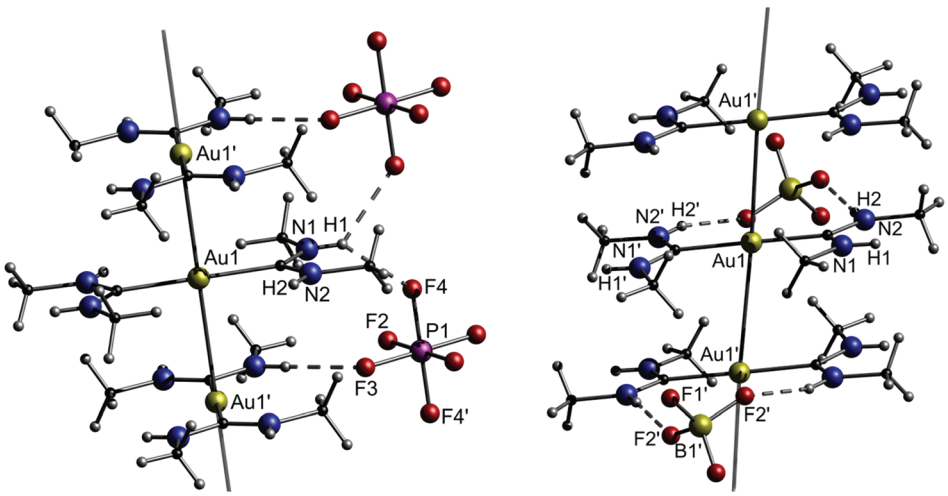

Fig. 5 Left: A portion of the structure of crystalline [Au{C(NHMe)$_2$}$_2$][PF_6]·0.5acetone (**1a**). Solvent molecules (acetone) are omitted. Right: A portion of the structure of crystalline [Au{C(NHMe)$_2$}$_2$][BF_4] (**1b**).[108]

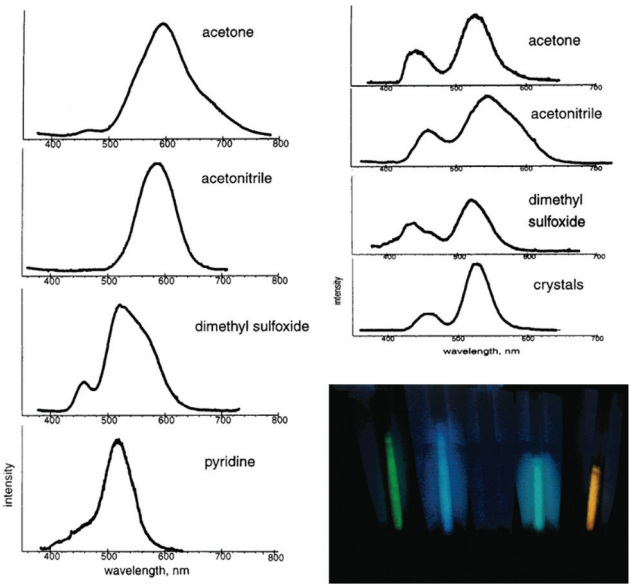

Fig. 6 Left: Emission spectra obtained from 6 mM solutions of **1a**, frozen at 77 K. Top right: Emission spectra obtained from 0.06 mM solutions of **1a** frozen at 77 K and crystalline **1a** at 77 K. Bottom right: Photograph of the luminescence from 6 mM solutions of **1a** at 77 K. From left to right: MeCN, DMSO, DMF, pyridine, acetone. Reprinted (adapted) with permission.[108] Copyright 2002 American Chemical Society.

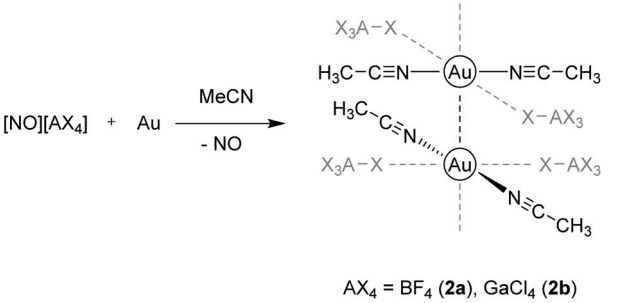

Scheme 2 Synthesis and molecular structures of compounds **2a** and **2b** in the solid state.[112]

luminescence properties. Note that the luminescence of **1b** is affected in a similar fashion by dissolution in the aforementioned solvents and the freezing procedure.

The absence of luminescence in solutions of **1a** is presumably due to a breakdown of the polymeric structure into smaller units or monomers. The fact that the emission spectra of the frozen solutions strongly resemble the spectrum of polycrystalline **1a** suggests similarities in the respective molecular structures. In this regard, it is reasonable that oligomeric forms of $[Au\{C(NHMe)_2\}_2][PF_6]$, generating species similar in structure to the arrangement of crystalline **1a**, do form upon freezing the different solutions. The detailed molecular structures that are present in the frozen solutions could not be resolved, but it is apparent that the luminescence behaviour is affected by the number of gold ions, the Au–Au distance, the orientation of the ligands, hydrogen bonding interactions, the anion itself and the coordination of solvent molecules to the metal centers.[111] A detailed understanding of these aspects might play a crucial role, *e.g.* in the development of sensors for different chemical environments.

Other examples for purely cationic chain links paired with weakly coordinating anions (WCA) were presented by the Krossing group in 2016.[112] A series of $[Au(MeCN)_2][WCA]$ salts was prepared by direct oxidation of elemental gold in acetonitrile (MeCN) with nitrosyl salts of the type $[NO]^+[WCA]^-$ ($[WCA]^- = [BF_4]^-$, $[GaCl_4]^-$, $[B(CF_3)_4]^-$, $[Al(OC(CF_3)_3)_4]^-$ and $[B(CF_3)_3CN]^-$). The resulting complexes $[Au(MeCN)_2][BF_4]$ (**2a**) and $[Au(MeCN)_2][GaCl_4]$ (**2b**) contain gold strings only composed of $[Au(MeCN)_2]^+$ cations that are interconnected by aurophilic interactions in the solid state, whereas the corresponding $[B(CF_3)_4]^-$ and $[Al(OC(CF_3)_3)_4]^-$ salts form dimers and monomers, respectively (Scheme 2).

In both **2a** and **2b**, a weak interaction to the fluoride and chloride atoms of the respective anions BF_4^- and $GaCl_4^-$ is observed in a *trans* 'coordination', although the atomic distances are outside of their van der Waals distance. In **2a**, the contact lengths between adjacent gold atoms follow a repeating medium–short–short–medium–long–long pattern with the shortest contact being 3.113 Å. The respective Au–Au distances in **2b** are equidistant (3.540 Å). Interestingly, Au–Au contact lengths are correlated with the coordination strength of the anions, which follows a $[BF_4]^- > [GaCl_4]^- > [B(CF_3)_4]^- > [Al(OC(CF_3)_3)_4]^-$ sequence.[113,114] The cations thus appear in four forms: (a) as a chain with strong contacts (**2a**), (b) as a chain with weak contacts (**2b**), (c) as a dimer ($[WCA]^- = [B(CF_3)_4]^-$) and (d) as a monomer ($[WCA]^- = [Al(OC(CF_3)_3)_4]^-$). This leads to the hypothesis that more electron-rich gold(I) centers feature stronger aurophilic interactions.

The assumption that the respective anion plays a decisive role regarding the molecular structure and resulting properties of cationic gold strings is further supported by a series of $[(C_6H_{11}NC)_2Au][XF_6]$ salts (X = P (**3a**), As (**3b**), Sb (**3c**)) published by the Balch group.[115–117] The hexafluoropnictogenates PF_6^-, AsF_6^- and SbF_6^-, although being weakly coordinating anions, alter the structure and thus the photophysical properties (including vapochromism and thermochromism) of the cationic string consisting of the two-coordinate $[(C_6H_{11}NC)_2Au]^+$. The term 'thermochromism' is used to describe a (typically reversible) temperature dependent change in the photophysical properties (*e.g.* colour or emission wavelength) of a sample. This phenomenon can be attributed to a change in the molecular or crystal structure.[118,119] Both compounds **3a** and **3b** crystallize either as colourless, blue-emitting crystals or as yellow, green emitting crystals. Interestingly, the colourless crystals of **3a** and **3b** are isostructural (Fig. 7, $P2_1/c$), whereas the yellow crystals exhibit different solid state structures (Fig. 7, $P2_12_12_1$ and $P\bar{1}$). The SbF_6^- derivative **3c** is obtained as pale-yellow crystals as well, exhibiting a blue luminescence, yet its molecular structure is entirely different from that of **3a** and **3b**. Two different chains of cations are

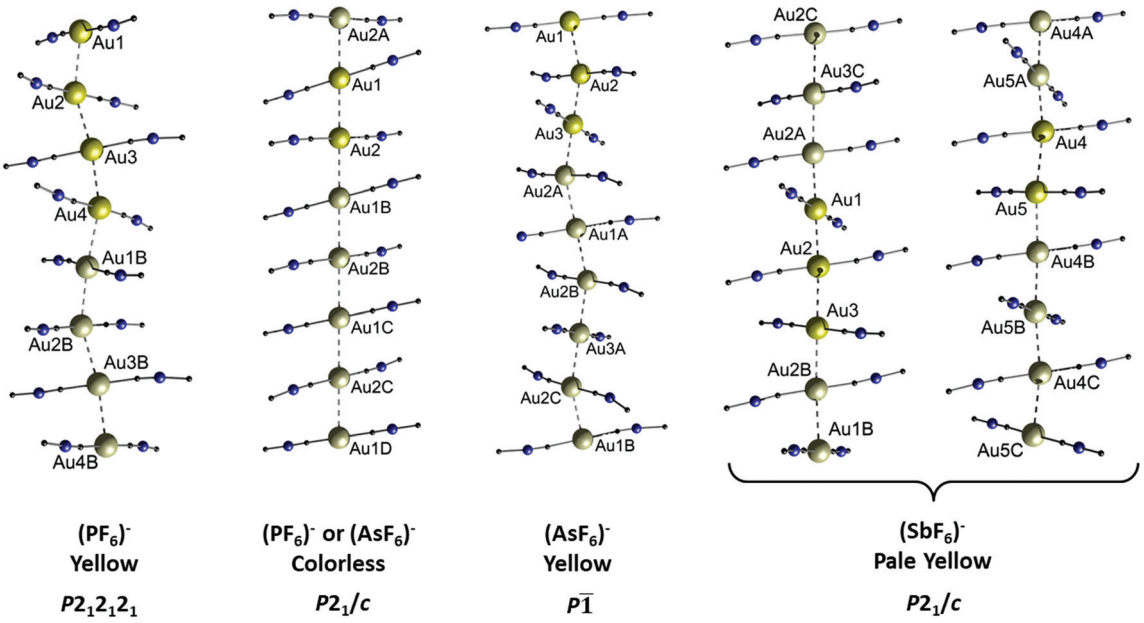

Fig. 7 Comparison of the columnar structures of the different forms of $[(C_6H_{11}NC)_2Au][XF_6]$ (X = P (**3a**), As (**3b**), Sb (**3c**)). For clarity, only the gold ions and the CNC portion of the ligands attached to the metals are indicated. Aurophilic interactions are shown as dashed lines. Anions are not shown. There are no solvate molecules in any of the crystal structures. Reprinted (adapted) with permission.[115] Copyright 2020 American Chemical Society.

observed and both run parallel along the same crystallographic axis (Fig. 7). The Au–Au separations of **3a–c** are summarized in Table 1.

Although being intensely luminescent in the solid state, solutions of **3a–c** are not emissive, which is consistent with a breakdown of the polymeric structure into monomers. However, upon exposure of the yellow, green-emitting polymorphs of **3a** and **3b** to vapours of selected solvents (dichloromethane, acetone, methanol or acetonitrile), a conversion to their respective colourless, blue-emitting polymorphs is observed (Fig. 8). In contrast, no change in colour or luminescence was observed in similar experiments with **3c**.

Crystalline samples of **3a–c** can be melted upon rising the temperature to a range of 113–126 °C. Independent of the polymorph type, the resulting melts of all samples are colourless and exhibit a bluish-white emission. Upon cooling, the respective yellow polymorphs of **3a** and **3b** are eventually formed, indicating that these are the thermodynamically more stable forms. Cooling the melt of **3c** results in the reformation of crystalline **3c**. However, a peculiarity is observed regarding the colourless polymorph of the AsF_6^- derivative **3b**, which, upon rising the temperature to 100 °C, transforms into a

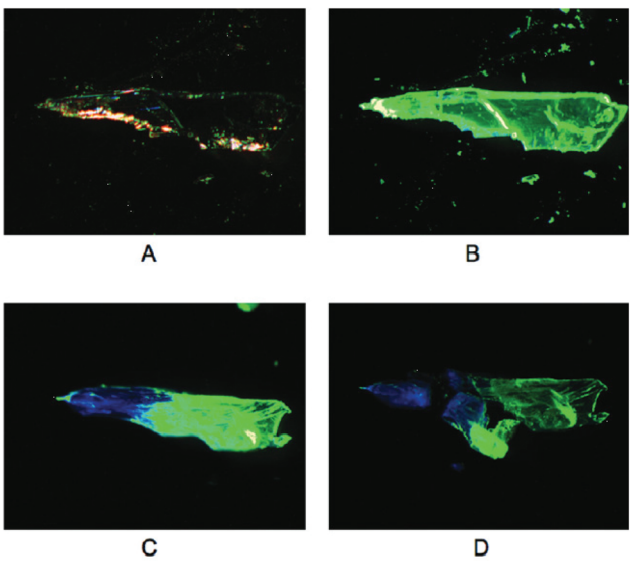

Fig. 8 Photographs of crystalline **3b**: (A) at ambient light, (B) upon UV irradiation, (C) after exposure to dichloromethane vapour upon UV irradiation, and (D) after crushing the crystal upon UV irradiation. Reprinted (adapted) with permission.[115] Copyright 2020 American Chemical Society.

Table 1 Au–Au separations of **3a–c** [115–117]

Sample	Colourless polymorph	Yellow polymorph
3a	3.1822(3) Å	2.9803(6) Å 2.9790(6) Å 2.9651(6) Å 2.9643(6) Å
3b	3.1983(8) Å	3.0230(5) Å 3.0097(6) Å
3c		Chain 1: 3.0252(7) Å 3.0858(7) Å Chain 2: 3.0424(9) Å 3.0782(9) Å

yellow solid without melting. The emission spectrum of this solid is nearly identical to that of the respective yellow polymorph. A similar yellow solid is formed by cooling the melt of **3b**, but in this case, the emission spectrum of this amorphous sample does not resemble the spectra of either the colourless or the yellow polymorph, indicating the formation of a new phase. The colourless polymorph of **3b** is the only sample that shows this thermochromic behaviour. In addition, the mixed-anion salts $[(C_6H_{11}NC)_2Au][PF_6]_{0.5}[AsF_6]_{0.5}$, $[(C_6H_{11}NC)_2Au][PF_6]_{0.5}[SbF_6]_{0.5}$, $[(C_6H_{11}NC)_2Au][AsF_6]_{0.5}[SbF_6]_{0.5}$, $[(C_6H_{11}NC)_2Au][PF_6]_{0.25}[AsF_6]_{0.75}$ and $[(C_6H_{11}NC)_2Au][PF_6]_{0.75}[AsF_6]_{0.25}$ were prepared by co-crystallization. Similar to **3a** and **3b**, colourless, blue-emitting and yellow, green-emitting polymorphs were found for all mixed-anion salts. Remarkably, all of the colourless crystals formed from a mixture of two anions show luminescence thermochromism below their melting points, similar to the colourless polymorph of **3b**. In the interest of an overall view, we would like to dispense a further detailed discussion about the mixed-anion salts, yet an in-depth investigation of these compounds can be found in the original work.[115] The thermochromic and melting point ranges are summarized in Table 2. A picture of the thermochromic behaviour is shown in Fig. 9.

Table 2 Thermochromic and melting point ranges[115]

Compound	Thermochromic range [°C]	Melting point range [°C]
Colourless form		
$[(C_6H_{11}NC)_2Au][PF_6]$	None	115–120
$[(C_6H_{11}NC)_2Au][AsF_6]$	98–102	123–125
$[(C_6H_{11}NC)_2Au][PF_6]_{0.5}[SbF_6]_{0.5}$	87–95	114–116
$[(C_6H_{11}NC)_2Au][AsF_6]_{0.5}[SbF_6]_{0.5}$	88–92	113–114
$[(C_6H_{11}NC)_2Au][PF_6]_{0.5}[AsF_6]_{0.5}$	104–108	118–119
$[(C_6H_{11}NC)_2Au][PF_6]_{0.75}[AsF_6]_{0.25}$	105–111	118–121
$[(C_6H_{11}NC)_2Au][PF_6]_{0.25}[AsF_6]_{0.75}$	100–105	118–121
Yellow form		
$[(C_6H_{11}NC)_2Au][PF_6]$	None	110–115
$[(C_6H_{11}NC)_2Au][AsF_6]$	None	123–126
$[(C_6H_{11}NC)_2Au][SbF_6]$	None	113–115

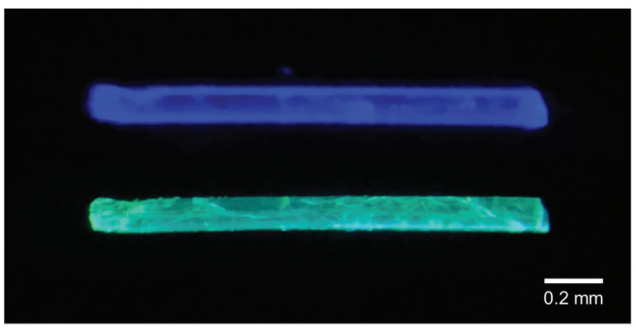

Fig. 9 Photographs of the luminescence from a crystal of $[(C_6H_{11}NC)_2Au][PF_6]_{0.5}[AsF_6]_{0.5}$. Top: Blue luminescence at ambient temperature. Bottom: Green luminescence after heating to 104–108 °C. Reprinted (adapted) with permission.[115] Copyright 2020 American Chemical Society.

These results show the significant impact of the respective anion on the aurophilic interactions, even though being weakly coordinating and well separated from the chains of gold ions that form the 1D molecular structure. Most likely, the differences in the volume of the anions are responsible for the variations in the solid state structures and ultimately, in the thermochromic and vapochromic responses.

Purely anionic chain links

In this part, the utilization of negatively charged aurates $[A\text{-}Au\text{-}A]^-$ as building blocks for the synthesis of gold strings is presented. Among the whole compound class of gold strings, including neutral and charged chains, an anion aggregation resulting in aurophilicity-linked oligomers or polymers is only observed 'in very special cases', as stated by H. Schmidbaur and co-workers in 2002, referring to their own investigations.[120] Consequently, studies of gold strings consisting of purely anionic chain links are rather scarce. Representative cations can be simple organic molecules like paraquat (*N*,*N*′-dimethyl-4,4′-bipyridinium or 'Me_2bipy'), as shown by the Guloy group in 1998.[121] They presented the crystal structure of $[Me_2bipy][AuI_2]_2$ (**4**), in which the diiodoaurate anions form a single 1D chain that does not interact with the staggered countercations $[Me_2bipy]^{2+}$ (Fig. 10). The respective Au–Au distances (3.3767(3) Å) are in the range of aurophilic interactions.

Another fascinating example for negatively charged chains is a series of bis(thiocyanato)aurates $[Au(SCN)_2]^-$ with varying countercations including Na^+ (**5a**), K^+ (**5b**), Rb^+ (**5c**), Cs^+ (**5d**), NH_4^+ (**5e**), NMe_4^+ (**5f**), $N(n\text{Bu})_4^+$ (**5g**) and PPh_4^+, introduced in 2004 and 2006 by the Elder group.[122,123] The phosphonium salt consists of isolated monomers, whereas the nearly isostructural alkali salts, as well as the NH_4^+ salt, form infinite linear gold strings with alternating long and short Au–Au distances along the chain. The NMe_4^+ salt forms a kinked chain of trimers and the $N(n\text{Bu})_4^+$ salt consists of isolated dimers (Fig. 11).

Polycrystalline samples of **5a–g** show photoluminescence upon UV excitation at cryogenic temperature (77 K) with emission maxima ranging from 506 to 710 nm (Table 3).

In the crystal structures of the gold string compounds **5b–5f**, alternating short and long Au–Au distances can be observed. Thus, their molecular structures can be described as

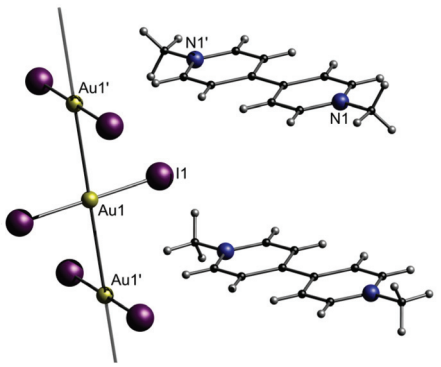

Fig. 10 Representation of the crystal structure of **4**.[121]

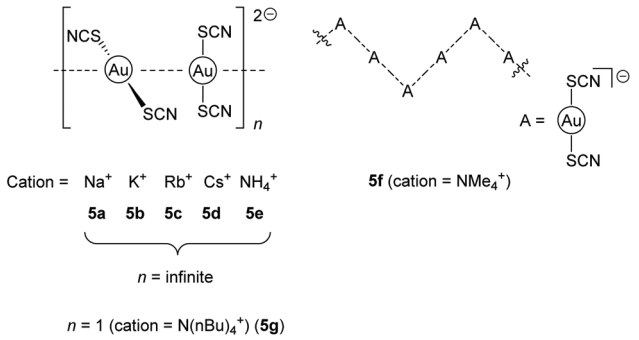

Fig. 11 Representation of the anion-arrangement in compounds **5a–g**.[122,123]

Table 3 Au–Au distances, excitation and emission wavelengths and corresponding energy of **5a–g** [122,123]

Sample	Au–Au [Å]	Exc [nm]	Em [nm]	E [cm^{-1}]
5b	3.0064(5) 3.0430(5)	320	516	19 379
5g	3.0700(8)	360	539	18 552
5c	3.0821(4) 3.1144(5)	320	506	19 762
5e	3.1409(3) 3.1723(3)	Not stated	627	15 949
5f	3.1794(2) 3.2654(2)	325	635	15 748
5d	3.2128(11) 3.2399(11)	320	670	14 925
5a	Unknown	320	710	14 084

a polymer of dimers (or trimers in the case of **5f**). Interestingly, when the emission energy (cm^{-1}) is plotted against the reciprocal of the short Au–Au bond lengths (Å^{-1}), a strong correlation can be observed (Fig. 12), which is in accordance with theoretical predictions.[124]

The overall length of the gold chains appears not to be a crucial factor in this case, as the dimeric complex **5g** and the assembly of trimers in **5f** fall in line with the data for the 'infinite' chains. Instead, it is very likely that not only the supramolecular string, but also single gold–gold pairs or 'Au_3' trimers with equidistant gold–gold contacts serve as the source of the emission.

A different picture emerges in ionic liquids containing $[Au(SCN)_2]^-$ moieties, when differently substituted imidazolium cations instead of 'inorganic' cations are used, as presented by Aoyagi and co-workers in 2015.[125] In this case, ionic liquids of the type $[C_n mim][Au(SCN)_2]$ (mim = methylimidazolium) are formed (Scheme 3).

The imidazolium salts **6b–d** are ionic liquids at ambient temperatures with very low glass transition temperatures around 200 K. An exception is compound **6a**, which forms a solid at room temperature. Compound **6a** consists of $[Au(SCN)_2]_n^{n-}$ gold strings with Au–Au distances of 3.1773(3) Å, as observed in the corresponding crystal structure (Fig. 13). Interestingly, using photocrystallography, it was possible to

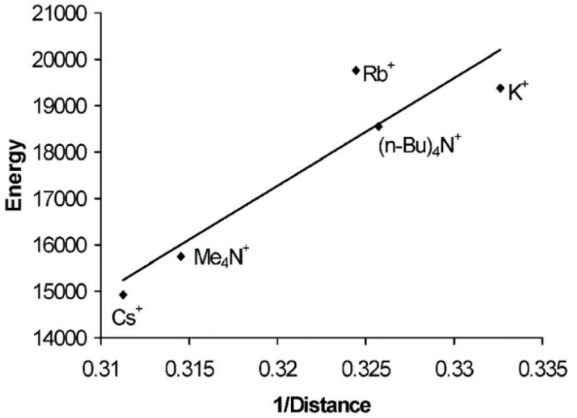

Fig. 12 Energy [cm^{-1}] *versus* 1/*d* [Å^{-1}] of the short Au–Au interaction of $[Au(SCN)_2]_n^{n-}$. Reprinted (adapted) with permission.[122] Copyright 2004 American Chemical Society.

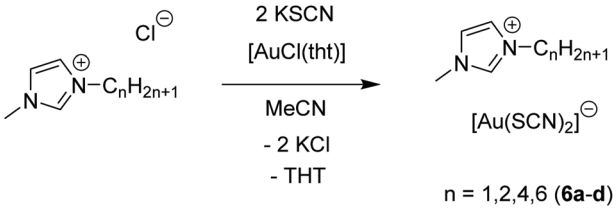

Scheme 3 Synthesis of **6a** and metal-containing ionic liquids (M-IL) **6b–d**.[125]

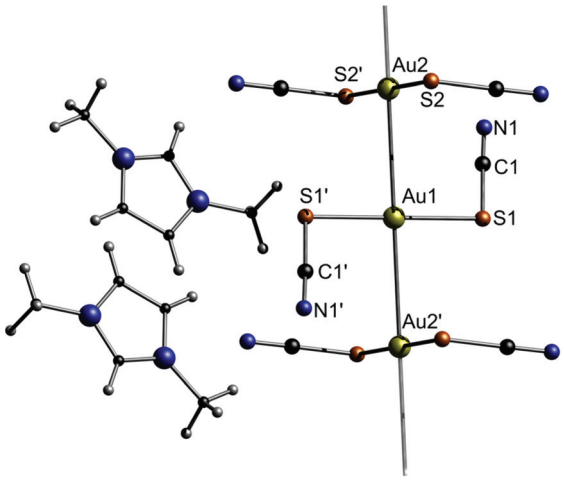

Fig. 13 Excerpt of the crystal structure of **6a**.[125]

resolve the structural changes induced upon UV light irradiation. Besides a change in the unit cell parameters, an excimeric contraction of the (Au–Au)* distance is observed as well. A list of changes regarding bond lengths is summarized in Table 4.

Furthermore, for the M-ILs **6b–d**, time-resolved laser fluorescence spectroscopy (TRLFS) was performed. The spectra of

Table 4 Changes of bond lengths in **6a** upon UV light irradiation (λ = 340 nm) at 100 K[125]

Bond	Lamp off [Å]	Lamp on [Å]	Δoff–on [Å]
Au1–S1	2.304(3)	2.319(5)	−0.015(6)
Au2–S2	2.294(2)	2.300(5)	−0.006(5)
S2–C2	1.680(10)	1.66(2)	0.02(2)
S1–C1	1.668(10)	1.65(2)	0.018(10)
Au1–Au2	3.1773(3)	3.1659(3)	0.0114(4)

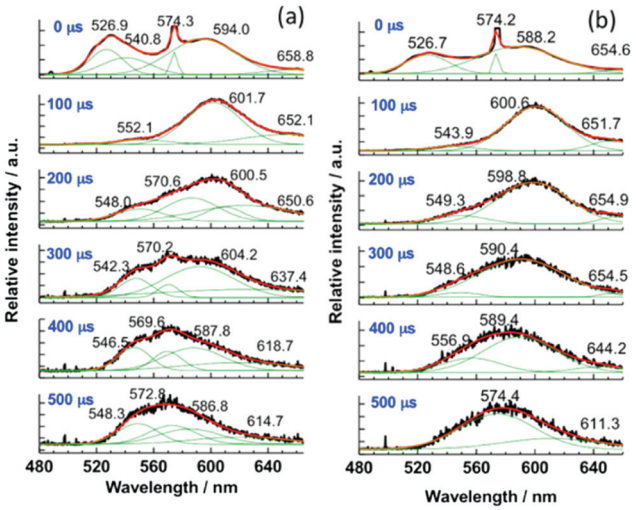

Fig. 14 Time-resolved luminescence spectra of **6b** (a), **6c** (b) and their deconvolution curves (green) at 77 K (λ_{ex} = 355 nm). Reprinted (adapted) with permission.[125] Copyright 2015 American Chemical Society.

the crude products are shown in Fig. 14. After a delay time of 100 µs to the excitation pulse, the peaks between 519 and 526 nm disappear, indicating fluorescence from the S_1 state, and all envelopes of the spectra undergo a blue-shift. The data indicate a colour change in a single luminescence decay event. The existence of multiple different aggregates of $[Au(SCN)_2]_n^{n-}$, possessing individual spectral features and luminescence lifetimes, is therefore suggested. For example, since the band gap of the T_1 phosphorescent state to the S_0 state is reduced by the number of metal ions involved, the peak in the deconvolution curves (green) at around 548 nm (Fig. 14, inset (a)) is attributed to a small aggregate, presumably a dimer $[Au(SCN)_2]_2^{2-}$, since the monomer (with no aurophilic interaction) shows no luminescence behaviour.

The dicyanoaurate anion $[Au(CN)_2]^-$ is a highly stable ion and is therefore used or observed in many different processes, such as cyanide leaching,[126] gold electroplating[127] or in protein crystallography as a phasing agent.[128] A number of crystallographically investigated compounds containing $[Au(CN)_2]^-$ are described in the literature. However, the aggregation of multiple $[Au(CN)_2]^-$ units seems disfavoured in terms of Coulomb repulsion. On the other hand, the low steric demand, the simple linear structure and not least the hydrogen bond acceptor ability of the cyanides facilitate a self-aggregation process.[129,130] In this context, the Attar and Balch groups investigated the formation and luminescence of dicyanoaurate strings comprising common ammonium counter cations.[131] Among the presented piperidinium $[C_5H_{10}NH_2][Au(CN)_2]$ (**7a**), pyrrolidinium $[C_4H_8NH_2][Au(CN)_2]$ (**7b**), 1,1-diphenylhydrazinium $[Ph_2NNH_3][Au(CN)_2]$ (**7c**) and tetrapropylammonium $[(C_3H_7)_4N][Au(CN)_2]$ (**7d**) salts, only the latter does not form a polymeric string in the solid state, presumably due to a lack of N–H groups suitable for hydrogen bonding to the cyanide moieties of the anions. Exemplarily, the crystal structure of **7c** is shown in Fig. 15.

In compound **7c**, the aurates form an infinite gold string with equidistant Au–Au separations of 3.0866(4) Å. It is noteworthy that hydrogen bonds between the cyanides and the 1,1-diphenylhydrazinium cations and additional water molecules stabilize and support the formation of the string compound. The crystal structures of the analogues **7a** and **7b** are comparable to that of **7c**, although hydrogen bonds are exclusively formed between the cyanide and the ammonium moieties.

In general, the Au–Au distances of **7a–c** are remarkably short and lie in a narrow range of 3.0795(4)–3.0969(3) Å, whereas the shortest metal–metal distance in the tetrapropylammonium derivative $[(C_3H_7)_4N][Au(CN)_2]$ (**7d**) is 7.526(1) Å and therefore far outside the aurophilic range. In consequence, crystalline **7a–c** show intense blue luminescence, even at ambient temperature. The small range of the emission maxima (436 nm (**7a**), 451 nm (**7b**) and 400 nm (**7c**)) reflects the fact that their molecular structures in the solid state and their respective Au–Au separations are similar. In contrast, the charge separated salt $[(C_3H_7)_4N][Au(CN)_2]$ without aurophilic contacts is non-luminescent at ambient and cryogenic (77 K) temperatures.

Purely anionic chains often include heterometallic compounds in which the chains are cross-linked by additional metal ions. By using dicyanoaurates $[Au(CN)_2]^-$ as anions, similar to compounds **7a–c**, but employing a metal complex as a $[cation]^+$, (hetero)bimetallic coordination polymers are obtained.[132] In this compound class, the bidentate character of the cyanide ligand is the driving force for the formation of supramolecular architectures. Representative compounds consist of $[M(L)_n]_x[Au(CN)_2]_y$ (M = Cu, Mn, Zn, Ni, Co, Cd, Au;

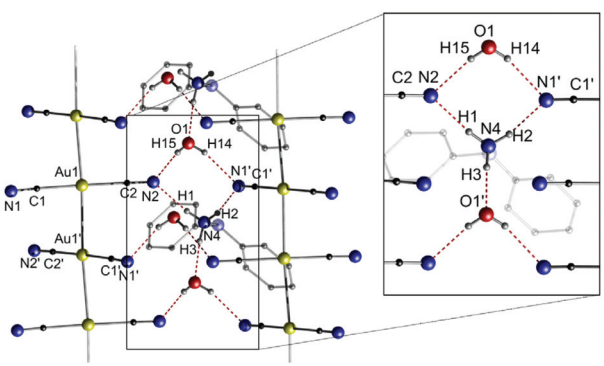

Fig. 15 Excerpt of the crystal structure of **7c**·H_2O.[131]

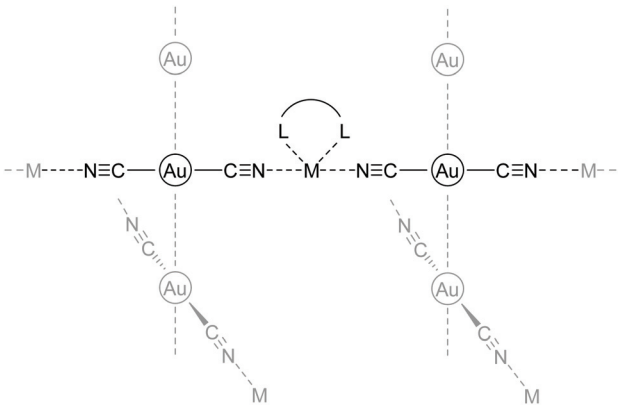

Scheme 4 General connectivity of heterometallic compounds with $[Au(CN)_2]^-$ as chain links.

L = multidentate N-donor ligand).[133–148] The general connectivity is illustrated in Scheme 4.

In many cases, the respective cationic $[M(L)_n]$ block consists of a divalent transition metal paired with a neutral multidentate ligand like phenanthroline, bipyridine or TMEDA. Additionally, +2 charged metal complex cations $[M(L)_n]^{2+}$, which consist of metal ions in higher oxidation states and negatively charged ligands, were employed for the construction of bimetallic coordination polymers, which tend to grow in two or three dimensions. The properties of the compounds, *e.g.* magnetism[142] or biological activity,[141] are mainly derived from the cationic $[M(L)_n]^{2+}$ building block. As an example, the first uranium-containing $[Au(CN)_2]^-$ coordination polymer $[UO_2(bipy)(MeO)(MeOH)]_2[(\mu\text{-}Au(CN)_2)(Au(CN)_2)]$ (**8**) was presented by Leznoff and co-workers in 2017 (Fig. 16).[149]

Compound **8** was synthesized by the reaction of $[NBu_4][Au(CN)_2]\cdot 0.5H_2O$, $UO_2(NO_3)_2\cdot 6H_2O$ and 2,2′-bipyridine in methanol. The molecular structure in the solid state consists of a one-dimensional gold chain structure of trinuclear $[UO_2(bipy)(MeO)(MeOH)]_2[Au(CN)_2]$ units linked by aurophilic contacts of 3.0528(5) Å to adjacent, unbound $[Au(CN)_2]^-$ units. The dicyanoaurate anions are staggered, with a C–Au–Au–C torsion angle of 75.1(6)°. The different stretching frequencies of the cyanide ligands can be observed in the IR spectrum ($\tilde{\nu}_{CN}$ = 2169 and 2133 cm^{-1}) as well as in the corresponding Raman spectrum ($\tilde{\nu}_{CN}$ = 2187 and 2148 cm^{-1}). The blue-shifted bands can be assigned to the uranyl-bound $[Au(CN)_2]^-$ units, whereas the resonance at lower energy is assigned to the free $[Au(CN)_2]^-$ units.

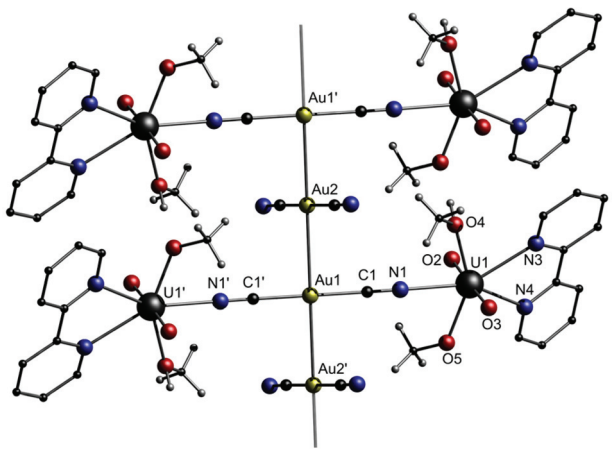

Fig. 16 Excerpt of the crystal structure of **8**.[149]

Gold strings with overall neutral chains

Alternating cationic and anionic chain links

In this part, gold chains comprising gold double salts are presented. The term 'double salt' is used to describe ionic species in which both cations and anions contain metal ions, although initially, it was primarily used in solid-state chemistry to refer to $(M)(M')(X)_n$ species such as $KAl(SO_4)_2\cdot 12H_2O$.[35] In case both ions are gold complexes, their aurophilic attraction is moreover supported by attractive Coulomb interactions.

In 2018, Lu, Chen and co-workers presented a library of 35 different combinations of $[Au(NHC)_2][MX_2]$ (NHC = N-heterocyclic carbene; M = Au or Cu; X = halide, cyanide or arylacetylide) complex salts (Fig. 17), outlining the large diversity of the double-salt approach.[15,150,151] Although not every compound was analysed by single crystal X-ray diffraction, it is assumed that all double salts feature infinite metal strings in the solid state. A representative crystal structure (**C3–A8**) is shown in Fig. 17. The intermetallic distances of the double salts, of which crystal structures were determined, are in the range of 3.182–3.384 Å (Au–Au) and 3.373–3.398 Å (Au–Cu). The prepared complex salts are emissive in the solid state upon UV irradiation with emission maxima ranging from 448 nm (**C1–A1**) to 785 nm (**C3–A14**), emission lifetimes ranging from 0.1 μs (**C3–A13**) to 7.1 μs (**C1–A2**) and quantum yields ranging from 10% (**C3–A10**) to 99% (**C1–A5** and **C2–A5**). A picture of selected double salts upon UV-irradiation and representative emission spectra are shown in Fig. 18.

The following structure–property relationships can be derived from in-depth analysis of the photophysical properties: (1) Maintaining the anion, the emission energy of the resulting double salt red-shifts with more electron withdrawing NHCs on the cations. (2) Maintaining the cation, the emission energy of the resulting double salt red-shifts with more electron donating ligands on the anion series of $[AuX_2]^-$, yet it remains constant for the respective $[CuX_2]^-$ salts. (3) The double salts of the form $[Au(NHC)_2][CuCl_2]$ generate the highest quantum yields.

Interestingly, the combinatorial pool of double salts allows for multi-colour emission by combining two phosphors with different emission colour. Therefore, co-crystallization of **C2**, **A1** and **A4** (molar ratio 2 : 1 : 1) results in the formation of the triple salt **C2–A1/A4** (Fig. 19).

The triple salt **C2–A1/A4** indeed shows dual emission at 586 and 652 nm. The latter is significantly red-shifted compared to the corresponding parent complex salts **C2–A1** (469 nm) and

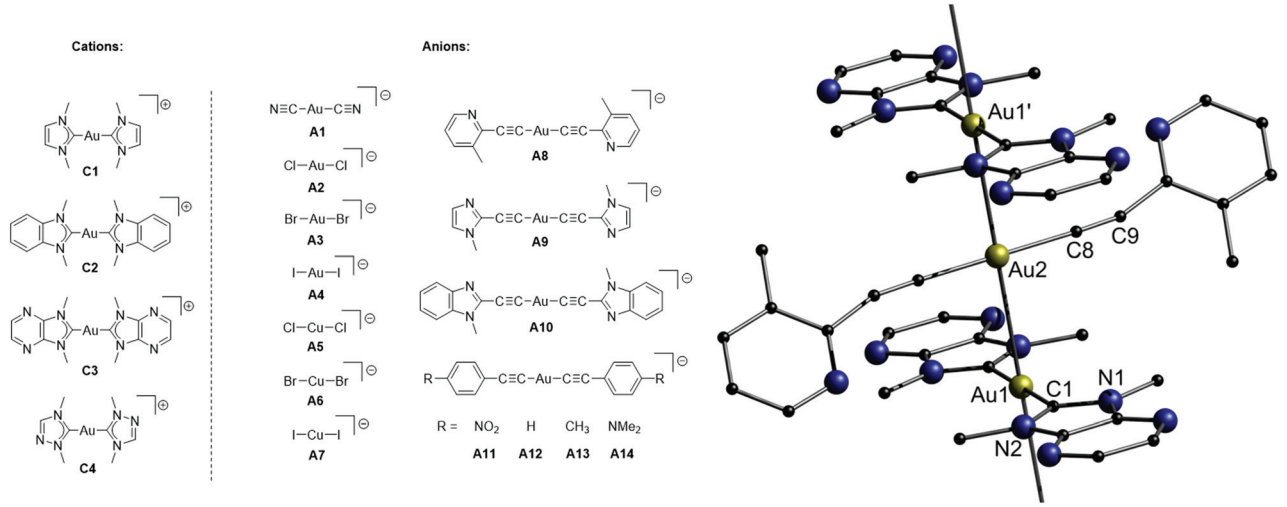

Fig. 17 Left: Chemical structures of four cationic (**C1–C4**) and fourteen anionic (**A1–A14**) precursors. Right: Representation of the crystal structure of the double salt **C3–A8**.[15]

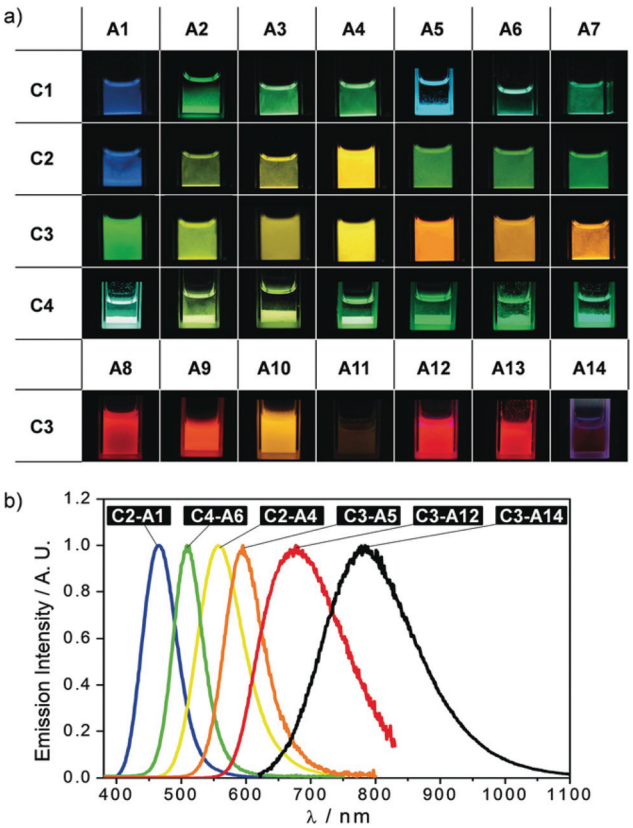

Fig. 18 (a) The images of the 35 complex salts dispersed in water or acetonitrile observed under a 365 UV lamp; (b) normalized solid-state emission spectra of selected complex salts showing the multi-colour luminescence. Adapted with permission from John Wiley & Sons, copyright 2018.[15]

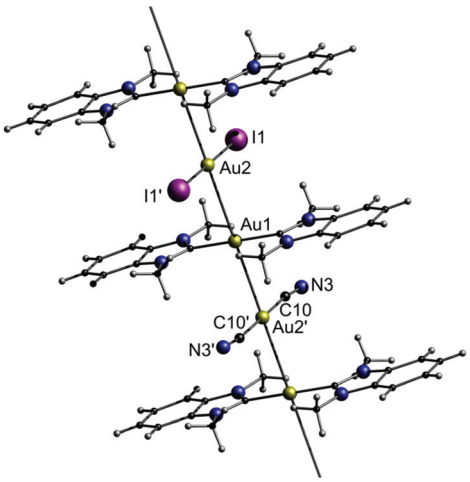

Fig. 19 Representation of the crystal structure of the triple salt **C2–A1/A4**.[15]

C2–A4 (570 nm), which can be explained by a simultaneous, yet not equal raise in energy of the HOMO and LUMO. This is due to a stronger σ-donating and weaker π-accepting capability of the iodide ligand in comparison with that of cyanide. The emission colour of **C2–A1/A4** can further be fine-tuned by varying the molar ratios of **A1** and **A4** upon co-crystallization (Fig. 20). By screening the combinatorial pool, Lu, Chen and co-workers impressively demonstrated that metallophilic interactions, in the form of 1D chains, provide an easy access to new phosphorescent materials with high quantum yields and versatile colour tunability.

Besides the combination of the typical monovalent cationic and anionic gold complexes[152,153] that were highlighted above, this concept can be readily expanded to mixed-valence gold(I/III) complexes,[154,155] as shown *e.g.* by Heck and co-workers.[156] A reaction of AuCl, $AuCl_3$ and cyclohexylcarbonitrile (NC-Cy) yielded the complex $[Au(NC\text{-}Cy)_2][AuCl_4]$ (**9**).

The crystal structure consists of linear gold strings with alternating $[Au(NC\text{-}Cy)_2]^+$ and $[AuCl_4]^-$ units (Fig. 21). The dis-

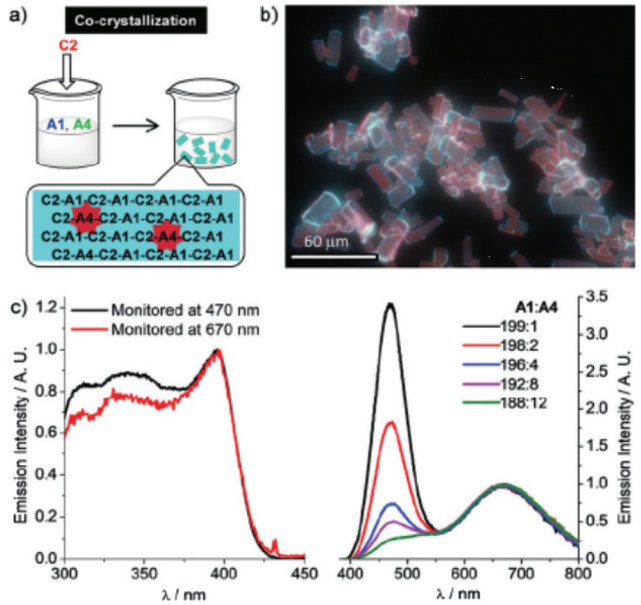

Fig. 20 (a) A sketch for the co-crystallization process; (b) fluorescence micrographs of **C2–A1/A4** microcrystals prepared *via* co-crystallization; (c) excitation and emission spectra of **C2–A1/A4** microcrystals with a variety of **A1** : **A4** ratios. Adapted with permission from John Wiley & Sons, copyright 2018.[15]

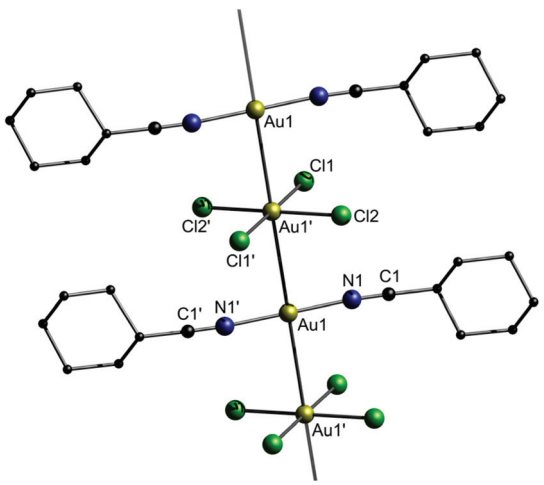

Fig. 21 Representation of the crystal structure of **9**.[156]

tances between the Au(I) and Au(III) centers are equidistant (polymorph A: 3.2382(4) Å; polymorph B: 3.2499(2) Å) and furthermore display the shortest unsupported Au(I)–Au(III) interactions that have been observed to date.

Neutral chain links

As shown in Fig. 4, gold strings with neutral chain links consist of neutral complexes, which form polymeric gold strings through unsupported aurophilic interactions.[157–171] As an example, Ecken *et al.* studied the effect of anions on the solid state structure of (*o*-xylyl isocyanide)gold(I) (Cl (**10a**), Br (**10b**), I (**10c**), CN (**10d**)).[172] Their study revealed that the Au–Au distances decrease in the order $I^- > Br^- > Cl^-$. For CN^-, which is a soft base as well, the Au–Au distances are similar to those of I^-. However, the trend differs from that of $[AuX(PMe_2Ph)]_2$ dimers and theoretical predictions, for which Au–Au distances decrease following a $Cl^- > Br^- > I^-$ sequence.[173–175] For **10a**, the presence of Cl^- anions results in the formation of dimers. In contrast, **10b** forms an asymmetric unit comprising two Au atoms linked by aurophilic interactions and setting off the third one aside, resulting in a slightly kinked chain (Fig. 22). Individual molecules of **10c** are aligned in chains through aurophilic interactions. **10d** also forms a structure similar to **10b**, but unlike **10c**, all three Au atoms in the asymmetric unit are involved in aurophilic interactions and thereby, a 2D structure is obtained. The intra- and interaggregate Au–Au distances are summarized in Table 5.

In accordance, Scheer and co-workers studied Au(I) complexes containing phosphanyl and arsanyl borane ligands and concluded that softer co-ligands coordinated to Au(I) tend to form extended polymeric structures due to multiple Au–Au interactions when compared to hard Lewis bases.[176] In fact, gold in its +I oxidation state is a very soft Lewis acid and therefore has a pronounced affinity towards soft bases such as sulfur or selenium,[177–180] which is in accordance with Pearson's principle of hard and soft acids and bases

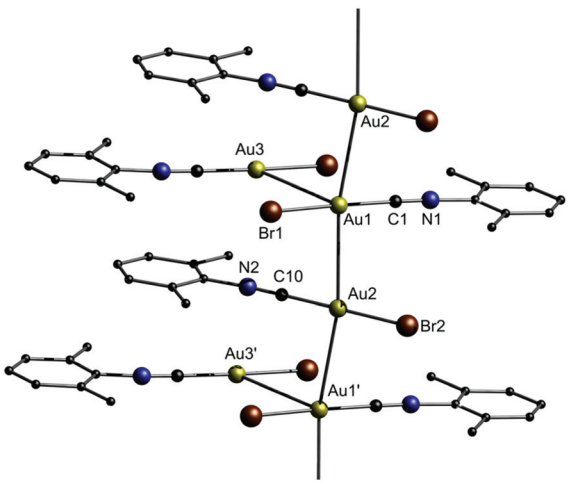

Fig. 22 Representation of the crystal structure of **10b**.[172]

Table 5 Variation of Au–Au separations with respect to the anions[172]

Sample	Intra Au–Au [Å]	Inter Au–Au [Å]	Solid-state structure
(*o*-xylylNC)AuCl (**10a**)	3.3570(11)	4.0225(12)	Dimers
(*o*-xylylNC)AuBr (**10b**)	3.3480(5)	3.7071(10)	Slightly kinked chain
(*o*-xylylNC)AuI (**10c**)	3.4602(3)	3.4602(3)	Slightly kinked chain
(*o*-xylylNC)AuCN (**10d**)	3.4220(6)	3.4615(6)	2D structure
	3.1706(4)		

(HSAB).[181–184] In this context, many gold string compounds are supported by bidentate dithiophosphate,[185–189] dithiocarboxylate,[190,191] diselenophosph(in)ate[192,193] or related ligand systems.[194–199] The Ch-X-Ch donor sites (Ch = chalcogenide, X = C, P) exhibit a low steric demand, which allows for the formation of gold strings comprising intermolecular connected homoleptic digold complexes (Fig. 23).

In 2014, Katrusiak and co-workers studied the behaviour of a dithiocarbamate-ligated one-dimensional gold string towards the application of pressure.[200] The two known polymorphs of $[Au(Et_2DTC)]_2$ (**11**) (DTC = dithiocarbamate) differ in their respective crystal structures as shown in Fig. 24. The α-phase consists of repeating identical units of $[Au(Et_2DTC)]_2$, whereas the β-phase exhibits an interval two times longer. For both, the intramolecular Au–Au bond lengths are about 2.78 Å, while the respective unsupported intermolecular Au–Au distance is about 0.2 Å longer.

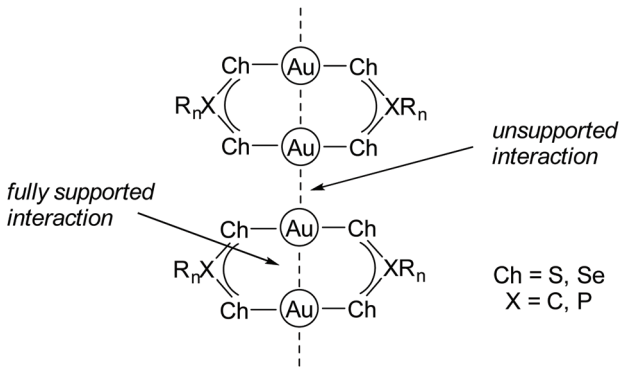

Fig. 23 General connectivity of gold strings comprising Ch-X-Ch ligand systems (Ch = chalcogenide, X = C, P).

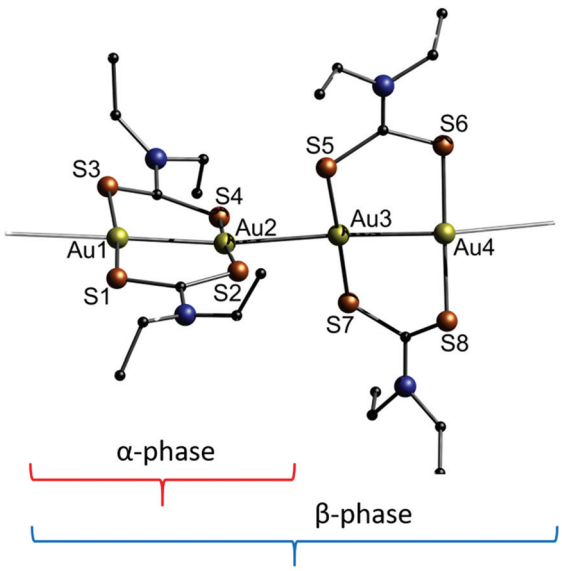

Fig. 24 Representation of the crystal structure of **11**. The brackets indicate the repeating unit of the two different polymorphs.[200]

The selective formation of either the α- or the β-phase can be controlled by varying the crystallization conditions or by the application of pressure. It is observed that above 50 MPa, the tetragonal crystals of the α-phase transform to an orthorhombic β-phase. Interestingly, the Au–Au distances can be further compressed by increasing the pressure. Thereby, the intermolecular Au–Au bonds are shortened at an average rate of −0.1006 Å per applied GPa. The average compressibility of the fully supported intramolecular Au–Au bonds, measured between 0.1 MPa and 1.0 GPa, is −0.0435 Å GPa^{-1} (Fig. 25). Thus, the fully supported bond is more than two times harder (*i.e.* deforms twice less). At 0.1 GPa, the supported Au–Au bonds are similar in length to that in metallic gold, whereas a pressure of 1.0 GPa diminishes the contact length to 2.72 Å, which therefore is about 0.05 Å shorter in comparison with that for the metal.

Another example for dithiocarbamate ligated gold strings involves the report of solvochromic luminescence regarding a dinuclear gold(I)-(aza-[18]crown-6)dithiocarbamate (**12**), as presented by Chao and co-workers.[201] The study investigates the effect of different solvates on the Au–Au distance of **12** and its resulting luminescence behaviour. Initially, the title compound was synthesized in the presence of MeCN to obtain **12**·2MeCN (Fig. 26).

Immersing the crystals of **12**·2MeCN in a *tert*-butylbenzene or *m*-xylene solution yielded **12**·*tert*-butyl-benzene·H_2O and **12**·0.5*m*-xylene respectively through single-crystal-to-single-crystal (SCSC) phase transformation. Hereby, **12** forms 1D chains irrespective of the presence of the aforementioned solvates. The Au–Au distances in **12**, when crystallized with different solvates and their corresponding emission wave-

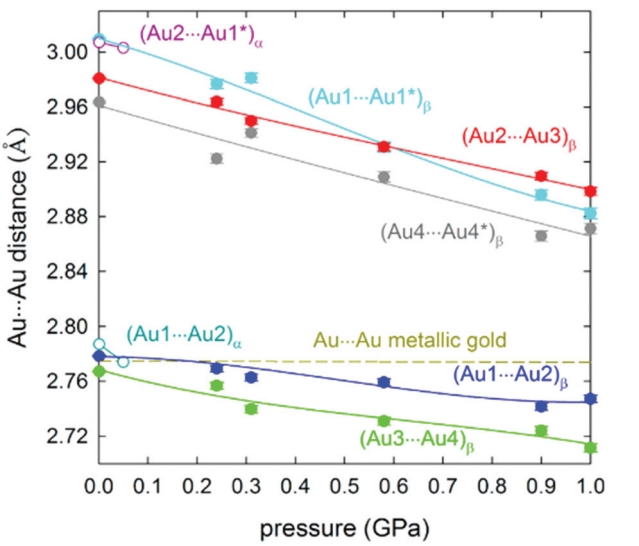

Fig. 25 Compression of the Au–Au distances in phases α (open circles) and β (full symbols) of **11**. The pressure dependence of the Au–Au distance (hardly changing to 1.0 GPa) in metallic gold is shown as the dashed line. Intramolecular and intermolecular bonds are shown. Reprinted with permission.[200] Further permissions to this material should be directed to the ACS.

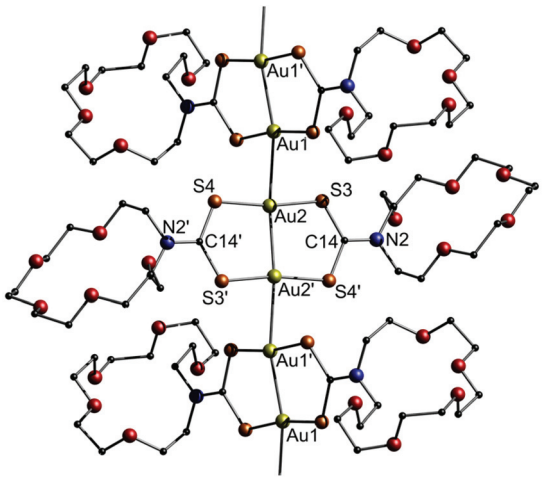

Fig. 26 Representation of the crystal structure of **12**·2(MeCN). Solvent molecules are omitted.[201]

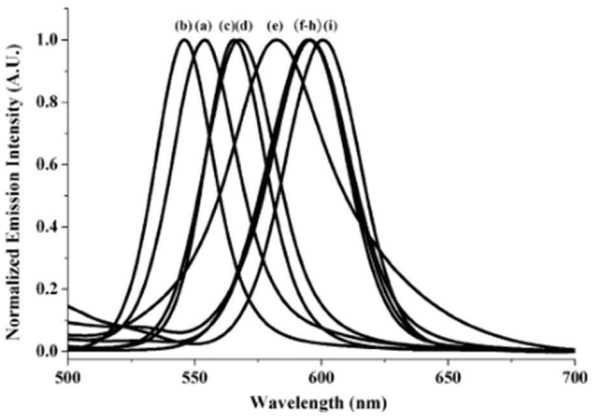

Fig. 27 Solvochromic luminescence (λ_{exc} = 380 nm) of (a) dry samples of **12**·2MeCN and upon grinding with (b) *tert*-butylbenzene, (c) benzene, (d) *p*-xylene, (e) *m*-xylene, (f) *o*-xylene, (g) anisole, (h) toluene, and (i) MeCN. Adapted with permission from John Wiley & Sons, copyright 2014.[201]

Table 6 Variation of Au–Au separations and emission wavelength with respect to different solvates[201]

Sample	Intra Au–Au [Å]	Inter Au–Au [Å]	Em [nm]
12·2MeCN	2.7186(3) 2.7249(3)	2.8355(3)	602
12·0.5*m*-xylene	2.755(2) 2.764(2)	2.890(2)–2.902(2)	583
12·^{t}Bu-benzene·H_2O	2.7713(4)	2.9420(5)	546
12 (dry sample)	Unknown	Unknown	553

Table 7 Photoluminescence data of **13a**, **13b** and respective daughter phases[23]

Sample	Em [nm]	Φ_{em} [%]	τ_{av} [μs]
13a	460 490	4	108
$\mathbf{13a_{SCSC}}$	566	16	5.33
13b	540	84	0.97
$\mathbf{13b_{SCSC}}$	535	6	13.8

lengths, are summarized in Table 6. From the values, a direct correlation between the Au–Au distance and the emission wavelength is observed. The study was extended to other aromatic solvates with electron donating groups and it was observed that the emission energies vary in the following order: *tert*-butylbenzene (546 nm) > dry (553 nm) > benzene (566 nm) > *p*-xylene (568 nm) > *m*-xylene (583 nm) > *o*-xylene, anisole, toluene (595 nm) > MeCN (602 nm). It is suggested that even though the electron-donating substituents in the solvates do not interact with the complexes, they influence stacking in the crystal lattice, affecting *i.e.* the Au–Au distance. As a result, the complexes exhibit distinct emission wavelengths as shown in Fig. 27. In a similar study, Ito and co-workers presented the formation of crystals comprising gold isocyanides as a versatile host system with guest-dependent luminescence.[202]

In 2016, Ito and co-workers reported the synthesis of phenyl(phenylisocyanide)gold(I) (**13a**) and phenyl(3,5-dimethylphenylisocyanide)gold(I) (**13b**), which exhibit mechano triggered SCSC phase transformations and possess interesting optical and electronic properties.[23,203–205] Complexes **13a** and **13b** were obtained as blue- and green-emitting single crystals respectively. However, a rapid phase transition was observed when the crystals were mechanically triggered. The phase transition of **13a** and **13b** propagated to the entire crystal to yield the daughter phases $\mathbf{13a_{SCSC}}$ and $\mathbf{13b_{SCSC}}$. The values determining the photoluminescence properties of the corresponding crystals are summarized in Table 7 and their respective PL spectra are displayed in Fig. 28. The PL spectra indicate that the phase transition induces a red- and blue-shift of the emission bands of **13a** and **13b**, respectively.

The changes in the emission properties were rationalized by the formation of different crystal structures (shown in Fig. 29).[23] The crystal structure of **13a** comprises dimeric units (formed by CH/π interactions) which are further stacked into 1D columns through additional CH/π interactions. The shortest Au–Au distance of 5.733 Å indicates the absence of aurophilic interactions. However, on mechanical stimulation, the monomeric units are twisted and aurophilic contacts of 3.177 Å are formed within the dimeric units of $\mathbf{13a_{SCSC}}$, which is in accordance with the red-shift of the emission band of **13a**. The crystal structure of **13b** consists of hexamers held together by aurophilic interactions, which are in the range of 3.274–3.112 Å. The hexamers are stacked into 1D columns supported by π–π interactions. Mechanical stimulation of the green-emitting species **13b** leads to the formation of the blue-emitting daughter phase $\mathbf{13b_{SCSC}}$ (the Au–Au distance is 4.784 Å) by disconnecting the aurophilic interactions. Additionally, weak CH/π interactions are formed in the daughter phase.

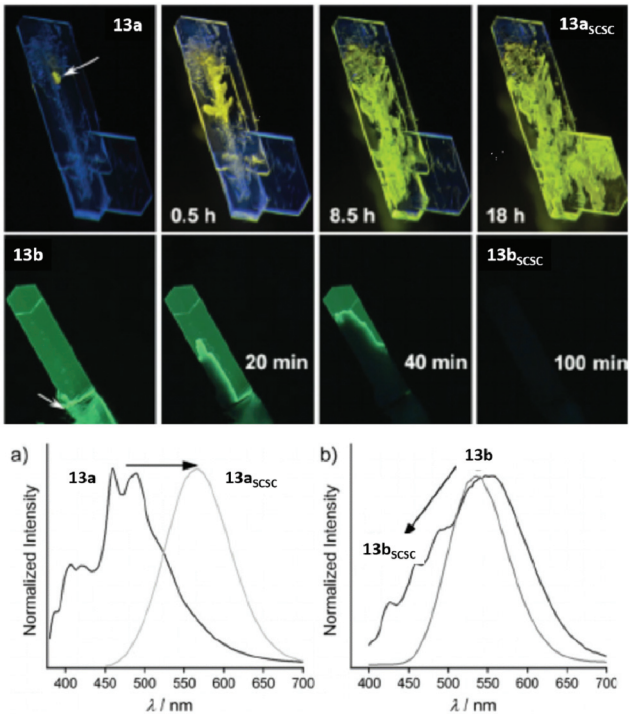

Fig. 28 Top: Mechano-triggered SCSC phase transition of **13a** to **13a**$_{SCSC}$ and **13b** to **13b**$_{SCSC}$ over time. Bottom: PL spectra of crystals **13a** and **13b** in comparison with their daughter phases obtained upon slight mechanical stimulation. Excitation wavelength: 365 nm. Adapted with permission from John Wiley & Sons, copyright 2016.[23]

Furthermore, intergrowth (IG) crystals comprising multiple crystal domains of different polymorphs were prepared by mechanical stimulation. Quantitatively, SEM images show the difference between the IG crystals and their respective daughter phases in terms of charging ability which is demonstrated in Fig. 30. Moreover, the conductive properties of the samples were analysed quantitatively. The evaluation of conductive properties typically requires an electrode–sample contact, which is not very effective for **13a** and **13b**, because such a contact would trigger SCSC phase transition. For this reason, flash-photolysis time-resolved microwave conductivity (FP-TRMC) measurements were performed. Although this method only gives insight into short-range (approx. 10 nm) conductivity, it is contactless and therefore suitable to increase the knowledge about the electronic properties of the polymorphs.

The maximum transient conductivity of species **13a** was determined to be $\varphi\sum\mu = 1.3 \times 10^{-5}$ cm^2 V^{-1} s^{-1}, while the conductivity of species **13a**$_{SCSC}$ was significantly higher at $\varphi\sum\mu = 1.3 \times 10^{-4}$ cm^2 V^{-1} s^{-1}. This increase of conductivity is most likely attributed to the formation of aurophilic interactions, as observed in the respective crystal structures (Fig. 29). For **13b** and **13b**$_{SCSC}$, maximum transient conductivities of 3.2×10^{-5} and 2.8×10^{-6} cm^2 V^{-1} s^{-1} were determined. The fact that the conductivity of **13b**$_{SCSC}$ is one order of magnitude lower than that for **13b** supports the assumption that the difference in conductivity of the samples is directly attributable to the presence or absence of aurophilic interactions in each species.

Another example focussing on the correlation between a change in the crystal structures and the photophysical properties due to external stimulation was presented by Eisenberg and co-workers in their report on luminescence tribochromism.[206] It describes the phenomenon that luminescence of suitable solid samples can be turned on by gentle grinding. Their work focussed on Au(I) thiouracilate complexes which were synthesized by reacting $[Au_2Cl_2(\mu\text{-dppm})]$ and $AgCO_2CF_3$

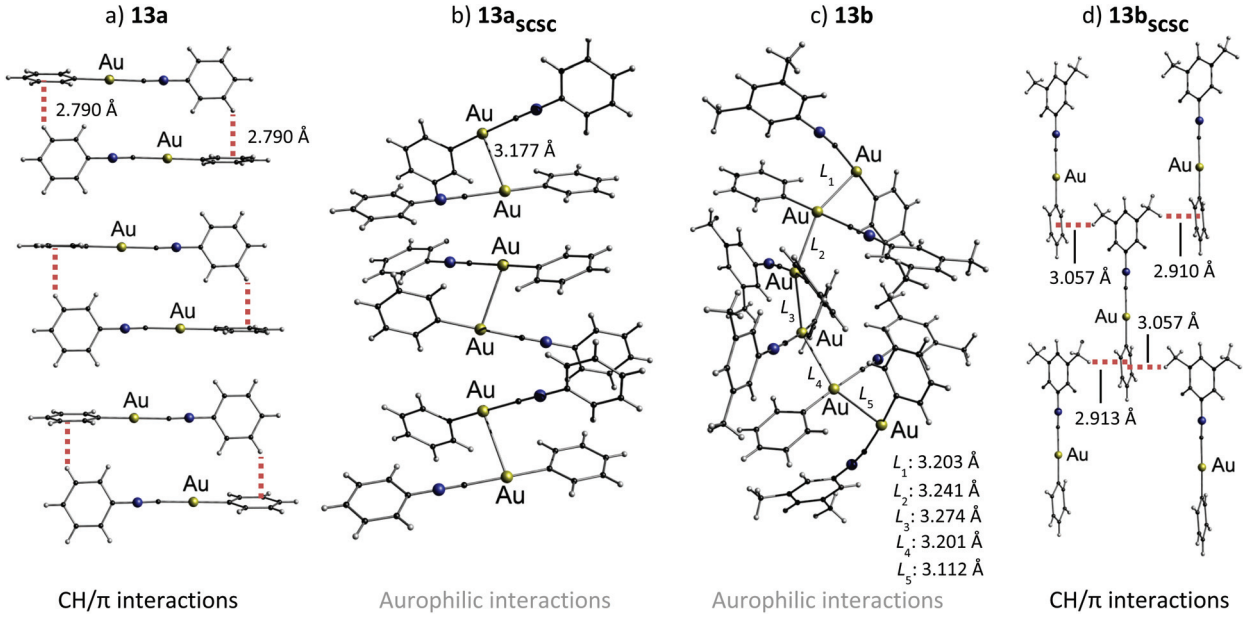

Fig. 29 Crystal structures of (a) **13a** (b) **13a**$_{SCSC}$ (c) **13b** and (d) **13b**$_{SCSC}$. Dotted lines and solid lines indicate CH/π interactions and aurophilic interactions, respectively.[23]

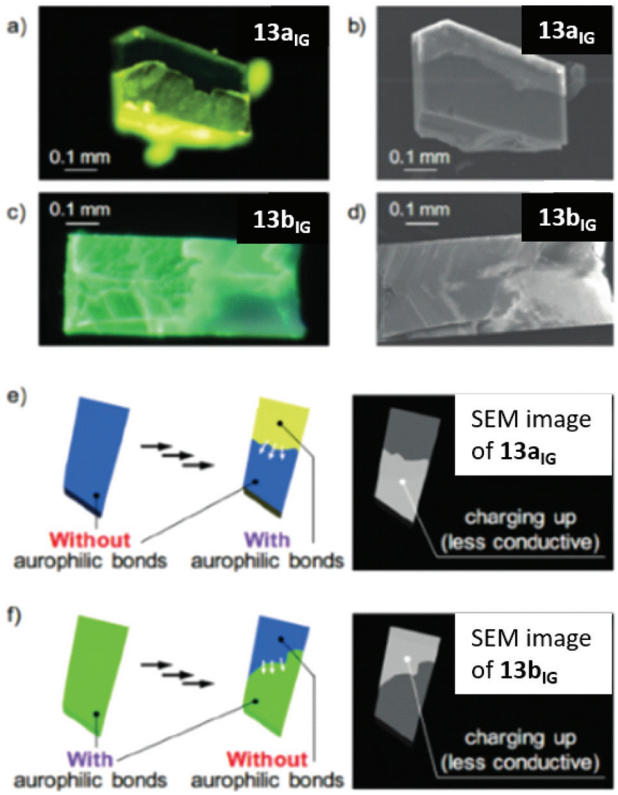

Fig. 30 Photoluminescence microscopy images of (a) **13a**$_{IG}$ and (c) **13b**$_{IG}$ upon excitation at 365 nm and sputtering-free SEM images of (b) **13a**$_{IG}$ and (d) **13b**$_{IG}$. Schematic representations of charging in (e) **13a**$_{IG}$ and (f) **13b**$_{IG}$, when observed by SEM. Adapted with permission from John Wiley & Sons, copyright 2018.[23]

with 2-thiouracil (TU) and 6-methyl-2-thiouracil (Me-TU) to give $[Au_2(\mu\text{-TU})(\mu\text{-dppm})]CF_3COO$ (**14a**) and $[Au_2(\mu\text{-Me-TU})(\mu\text{-dppm})]CF_3COO$ (**14b**), respectively (Scheme 5).

The obtained complex **14a** is a monocationic dinuclear Au(I) complex, which forms a helical structure in the solid state. A head to tail arrangement of the TU moieties is observed and an intramolecular Au–Au distance of 2.8797(4) Å and an intermolecular Au–Au distance of 3.3321(5) Å were determined. The structure of **14b** is similar to that of **14a**, except that the helix is discontinuous for head to head arrangement with an inter Au–Au distance of 4.344 Å and for the head to tail arrangement, the average Au–Au distance is 3.236–3.354 Å. **14a** and **14b** are either weakly luminescent or non-emissive. However, on gently grinding the solids, a bright cyan coloured luminescence was observed at room temperature. Recrystallization of the emissive forms in the presence of CF_3COOH again results in the formation of **14a** or **14b**. However, the emissive forms (**15a** and **15b**) can be selectively prepared by stirring CH_2Cl_2/MeOH solutions of **14a** or **14b** over Na_2CO_3 followed by filtration. The changes seen in the presence of the base/acid might be due to the deprotonation/protonation of the pyrimidine N–H moiety of thiouracil. The PL spectra of both emissive (**15b**) and non-emissive (**14b**) forms are displayed in Fig. 31.

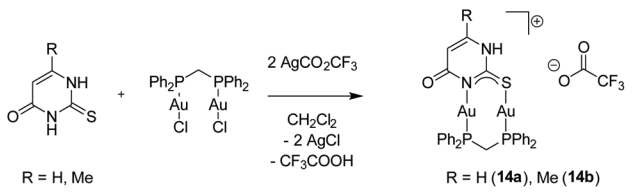

Scheme 5 Synthesis of **14a** and **14b**.[206]

The emissive compound **15b** has a similar structure to **14a** and **14b** but different packing arrangements, and comprises strong intermolecular aurophilic interactions between the dimers with a distance of 2.9235(4) Å (Fig. 32). Hence, it can be concluded that the delicate balance between changes in the Au–Au interactions and acidity of the sample results in this fascinating luminescence tribochromism.

Among the compound class of neutral gold strings, cyclic trinuclear gold complexes represent a special case as they exhibit unique electronic properties.[207] Their properties are majorly impacted by intermolecular interactions in the solid state that involve aurophilic contacts between the trimers.[208] Balch and co-workers have reported on the synthesis and intermolecular interactions in the polymorphs of $[Au_3(MeN{=}COMe)_3]$ (**16a**), $[Au_3(n\text{-PentN}{=}COMe)_3]$ (**16b**) and $[Au_3(i\text{-PrN}{=}COMe)_3]$ (**16c**) in 2005 (Fig. 34).[209] The trinuclear gold complexes of the form $[Au_3(RN{=}COR')_3]$ stack in four different arrangements, dependent on the bulkiness of the ligand substituents (R, R′), which retard or enhance intertrimer interactions, as reported by Omary and co-workers (Fig. 33). The stacking arrangements mainly differ regarding the nature of relative disposition of trimers with respect to each other.[24]

16a forms three polymorphs, namely hexagonal, monoclinic and triclinic. The hexagonal polymorph forms the stack arrangements **I** and **II**, while the triclinic and monoclinic poly-

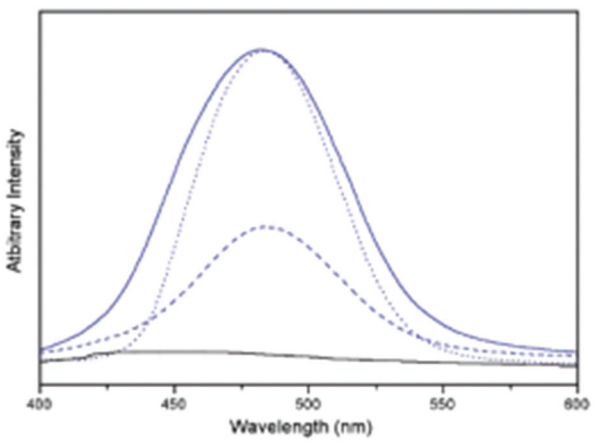

Fig. 31 Emission spectra of **14b** (black line) and ground crystals of **14b** (blue line), CH_2Cl_2 solution of **14b** (---) and crystals of **15b** (···) (prepared by reaction with Na_2CO_3) at room temperature (at λ_{ex} = 375 nm). Reprinted (adapted) with permission.[206] Copyright 2003 American Chemical Society.

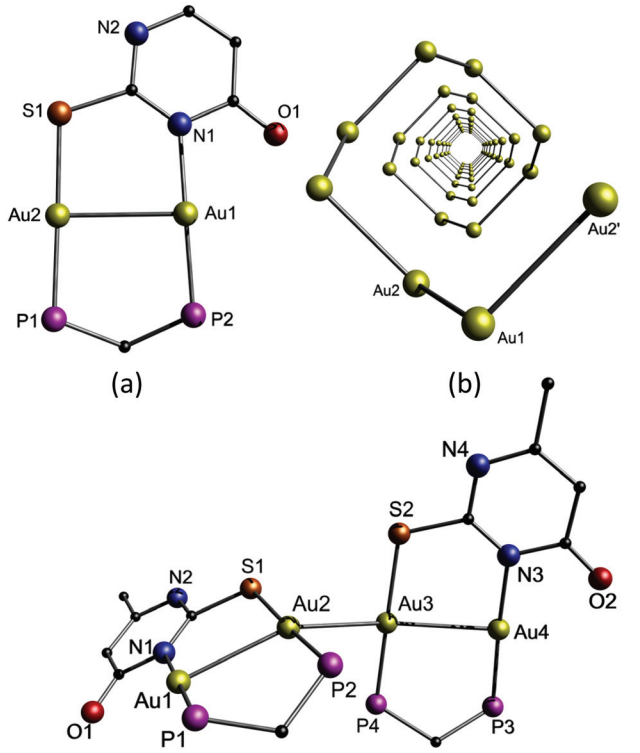

Fig. 32 Top: (a) View of cationic **14a** with phenyl rings omitted; (b) helical arrangement of the gold ions in **14a** with ligands omitted for clarity. Bottom: Perspective view of **15b** with phenyl rings omitted.[206]

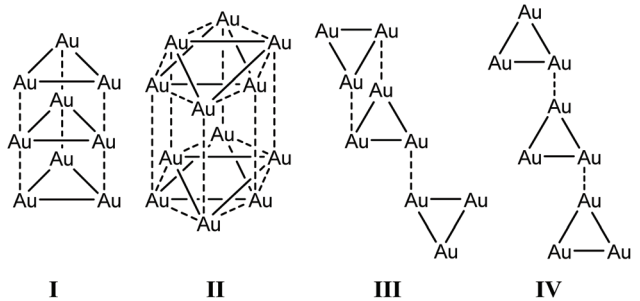

Fig. 33 Different stacking arrangements of trimers, in which the dashed lines and solid lines indicate inter and intramolecular Au–Au interactions. I, II, III and IV represent eclipsed, disorder staggered, chair and staircase stacking arrangements.[24]

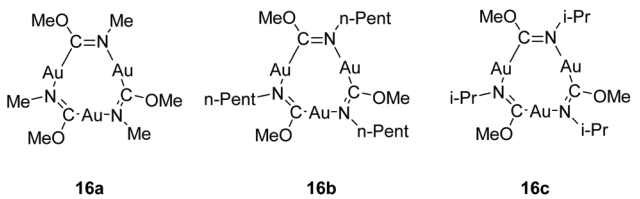

Fig. 34 Chemical structure of trinuclear Au(I) carbeniate complexes.[209]

Table 8 Variation of Au–Au separations and emission wavelengths in different polymorphs of **16a** [209]

Polymorph of **16a**	Intra Au–Au [Å]	Inter Au–Au [Å]	Em [nm]
Hexagonal I	3.308	3.346	450
Hexagonal II	3.280	3.384	520
Triclinic III	3.339	3.528	444
Monoclinic IV	3.323	3.653	431

morphs are present in the structural motifs **III** and **IV**, respectively. The Au–Au distances of the different polymorphs are summarized in Table 8. The hexagonal polymorphs of **16a**, in which extended, linear chains of gold ions are present, show some remarkable photophysical properties. Upon irradiation with near-UV light, a dual emission, consisting of a short-lived ($t \approx 1$ ms) emission at 446 nm and a broad long-lived (triexponential, $t \approx 1.4$, 4.4 and 31 s) emission at 552 nm, is observed. The yellow emission at 552 nm is readily detected by the human eye even seconds after the irradiation has stopped. Interestingly, if a suitable solvent (chloroform, dichloromethane, toluene, methanol, hexane, water) is dropped onto previously irradiated and still glowing crystals of **16a**, a bright burst of yellow light is observed. No overall chemical transformation appears to be involved in this solvoluminescence process. This phenomenon can be reproduced until the sample is entirely dissolved. For comparison, the sterically more demanding derivative $[Au_3(C_6H_5CH_2N{=}COMe)_3]$, which consists of separated individual molecules in the solid state, does not show long-lived luminescence behaviour. Consequently, the extended supramolecular aggregation of **16a** is believed to be important for the energy storage within the solid and may be involved in the solvoluminescence process. In this context, the recombination of a charge or electron separation may be responsible for the emission that occurs by exposure to the solvent.[94]

Moreover, the unique electronic characteristics of hexagonal **16a** are further demonstrated by the successive oxidation with molecular bromine or iodine, yielding in $[Au_3X_n(MeN{=}COMe)_3]$ (X = Br, I), where n is 2, 4 or 6.[210] A study of the electrochemical oxidation of this compound was presented as well.[211] In a 0.1 M $N(n\text{Bu})_4ClO_4$ dichloromethane solution as the supporting electrolyte, **16a** was oxidized at +650 mV, accompanied by the formation of fine, needle-like crystals on the electrode. Not suitable for single crystal XRD measurements, their composition was determined by bulk electrolysis and quartz crystal microbalance techniques to be $[Au_3(MeN{=}COMe)_3][ClO_4]_{0.34}$, being the first partially oxidized extended linear chain gold complex. It is assumed that the molecular structure of $[Au_3(MeN{=}COMe)_3][ClO_4]_{0.34}$ resembles the hexagonal polymorph of **16a**. Chronoamperometric studies confirmed this new phase to be conductive, which offers further insight into the solvoluminescence, energy storage and electron mobility along chains of gold complexes.

The *n*-pentyl substituted compound **16b** crystallizes in an orthorhombic (**16b-1**) and a triclinic polymorph (**16b-2**). **16b-1**

exhibits a stair case arrangement, in which the intermolecular Au–Au distance between the trimers is 3.618 Å, whereas the intramolecular Au–Au distances are 3.315(3), 3.260(2) and 3.332(2) Å. **16b-2** comprises four independent trimers in the asymmetric unit linked by aurophilic interactions (Au–Au: 3.4614(6), 3.3458(6), 3.6126(6) Å). The shortest Au–Au distance between the asymmetric units is 3.8125(6) Å. Among both polymorphs only **16b-2** is luminescent at room temperature with an emission band at 654 nm (excitation at 326 nm), resulting in a large Stokes shift. This indicates the possible occurrence of a metal-centered excimeric emission due to the contraction of the ground-state aurophilic association.[24] The structure of **16c** comprises only one trinuclear unit in the asymmetric unit. However, the shortest Au–Au distance in the trimers is 6.417 Å, which is far outside the aurophilic range. Moreover, **16c** is not luminescent at ambient temperature, most likely due to the absence of aurophilic interactions. Furthermore, it is suggested that steric effects of the side groups (R, R′) influence the formation of Au–Au interactions and thereby the photophysical properties.

Omary and co-workers have also reported their research on cyclotrimeric gold(I) carbeniates, $[Au_3(RN{=}COR')_3]$ (**17a**: R = Me, R′ = ^{n}Bu; **17b**: R = ^{n}Bu, R′ = Me; **17c**: R = R′ = ^{n}Bu and **17d**: R = cyclo-pentyl, R′ = Me).[24] The crystal structure of $[Au_3(MeN{=}CO^nBu)_3]$ (**17a**) is exemplarily shown in Fig. 35.

Their study revealed that a substitution of R or R′ leads to an alteration in solid-state stacking of the trinuclear units and thereby affecting opto-electronic and electronic properties. Bulky R and R′ groups tend to lie above or below the plane of the trinuclear units, which makes stacking of trinuclear Au units into 1D polymeric chains difficult. Molecular simulations of $[Au_3(HN{=}COH)_3]$ reveal that infinitely extended chains of eclipsed trinuclear units with head to tail arrangement tend to have smaller Stokes shifts and lower band gaps and reorganization energies (λ), which are ideal characteristics required for the design of semiconducting materials for molecular electronic devices.

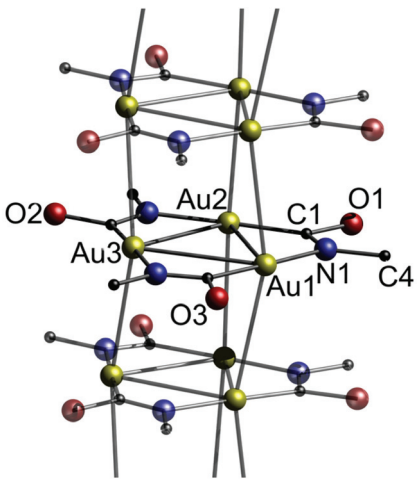

Fig. 35 Excerpt of the crystal structure of **17a** with *n*-butyl groups omitted for clarity.[24]

Table 9 Reorganization energies of different trinuclear complexes[24]

Sample	λ [eV]
$[Au_3(NH{=}COH)_3]$	0.448
$[Au_3(MeN{=}COMe)_3]$	0.664
$[Au_3(MeN{=}CO^nBu)_3]$	0.696

Charge transport properties of organic semiconductors in principle depend on the coupling between the geometric and electronic structures of the respective molecules.[212] The degree of chain orders in polymers and solid-state stacking in crystals majorly impact the charge transport ability in the organic molecules.[213,214] According to Marcus theory, the electron transfer rate (k_{et}) can be expressed as

$$k_{et} = \frac{4\pi^2}{h}\frac{1}{\sqrt{4\pi\lambda k_B}}t^2 \exp\left(-\frac{\lambda}{4k_B t}\right) \quad (2)$$

where T, k_B, and h represent temperature, Boltzmann's constant, and Planck's constant, respectively.[215–217] The equation is dependent on two important factors, the intermolecular transfer integral (t) and the intramolecular reorganization energy (λ). DFT studies predict that efficient solid-state packing in the form of extended chains and short intermolecular distances (as seen in $[Au_3(MeN{=}COMe)_3]$) facilitates strong electronic coupling and results in significant t values.[218] The λ value varies with the change in R and R′ groups as reported by Omary and co-workers (Table 9).

The molecular simulations predict that, if extended chains of $[Au_3(RN{=}COR')_3]$ with non-bulky groups can be synthesized, they can probably act as ideal semiconductor materials for fabricating molecular electronic devices.

Conclusions and perspective

The compound class of molecular gold strings is presented in this review. Their unique characteristic is their periodicity, which makes them valuable from synthetic and fundamental points of view. The physical properties of the strings are derived from the distance between adjacent gold ions and the electronic nature of the supporting ligands. The exposure to different external stimuli such as temperature, solvent interaction or mechanical stress alters the Au–Au distance, which goes along with a change in the physical properties. This is primarily demonstrated in the respective photoluminescence characteristics, as the emission energies typically decrease with larger metallic distances. Furthermore, the overall length of the gold strings is an important factor for the electronic structure, as observed *e.g.* by TRLFS measurements. Studying these structure–property correlations can help researchers to understand the nature of the aurophilicity phenomenon and to further develop potential applications. In this regard, the most interesting features certainly are their luminescence

behaviour and electronic properties. In the case of luminescence, the development and application of smart sensor materials, which *e.g.* are already known for lanthanide-based compounds[219,220] or molecular switches, which to date are majorly based on organic compounds,[221] are the next logical steps. In addition, by controlling the Au–Au distance of molecular gold strings and utilizing ligands with tailor-made electronic properties, emitters with predictable and tuneable emission wavelengths might be developed and used *e.g.* for OLED materials,[222] as it is already the case for copper and iridium complexes.[223–227] Another interesting aspect of molecular gold strings is their energy storage and conductive behaviour, as shown by the Balch, Omary and Ito groups,[23,24,211] making them promising candidates for molecular wires. The synthetic approaches towards molecular metal-containing wires and comprehensively understanding their electric characteristics have been in the focus of materials science for decades.[9,11,228] As a consequence, addressing these research opportunities is only possible by a multidisciplinary approach involving experimental and theoretical scientists.

Conflicts of interest

There are no conflicts to declare.

Acknowledgements

This review was written during the SARS-CoV-2 pandemic. We would like to thank all frontline workers and people who keep our society running.

The DFG funded Research Training Group (RTG) 2039 (Molecular architecture for fluorescence cell imaging) is acknowledged for financial support.

Notes and references

1 Z. Allahyari and A. R. Oganov, *npj Comput. Mater.*, 2020, **6**, 55.
2 Y. Kopelevich and P. Esquinazi, *Adv. Mater.*, 2007, **19**, 4559–4563.
3 B. Partoens and F. M. Peeters, *Phys. Rev. B: Condens. Matter Mater. Phys.*, 2006, **74**, 075404.
4 I. Szleifer and R. Yerushalmi-Rozen, *Polymer*, 2005, **46**, 7803–7818.
5 N. Todorova, A. J. Makarucha, N. D. M. Hine, A. A. Mostofi and I. Yarovsky, *PLoS Comput. Biol.*, 2013, **9**, e1003360.
6 T. Nakanishi, W. Schmitt, T. Michinobu, D. G. Kurth and K. Ariga, *Chem. Commun.*, 2005, 5982–5984.
7 R. Nadiv, G. Shachar, S. Peretz-Damari, M. Varenik, I. Levy, M. Buzaglo, E. Ruse and O. Regev, *Carbon*, 2018, **126**, 410–418.
8 J. N. Tiwari, R. N. Tiwari and K. S. Kim, *Prog. Mater. Sci.*, 2012, **57**, 724–803.
9 K. Jang, I. G. Jung, H. J. Nam, D.-Y. Jung and S. U. Son, *J. Am. Chem. Soc.*, 2009, **131**, 12046–12047.
10 R. Hayoun, D. K. Zhong, A. L. Rheingold and L. H. Doerrer, *Inorg. Chem.*, 2006, **45**, 6120–6122.
11 I.-W. P. Chen, M.-D. Fu, W.-H. Tseng, J.-Y. Yu, S.-H. Wu, C.-J. Ku, C.-h. Chen and S.-M. Peng, *Angew. Chem., Int. Ed.*, 2006, **45**, 5814–5818.
12 C.-C. Chiu, M.-C. Cheng, S.-H. Lin, C.-W. Yan, G.-H. Lee, M.-C. Chang, T.-S. Lin and S.-M. Peng, *Dalton Trans.*, 2020, **49**, 6635–6643.
13 J. M. Tour, *Acc. Chem. Res.*, 2000, **33**, 791–804.
14 I. P.-C. Liu, C.-h. Chen and S.-M. Peng, *Bull. Jpn Soc. Coord. Chem.*, 2012, **59**, 3–10.
15 Q. Liu, M. Xie, X. Chang, S. Cao, C. Zou, W.-F. Fu, C.-M. Che, Y. Chen and W. Lu, *Angew. Chem., Int. Ed.*, 2018, **57**, 6279–6283.
16 I. R. Whittall, M. G. Humphrey and D. C. R. Hockless, *Aust. J. Chem.*, 1997, **50**, 991–998.
17 J. Vicente, M. T. Chicote, M. D. Abrisqueta, P. González-Herrero and R. Guerrero, *Gold Bull.*, 1998, **31**, 83–87.
18 S. J. Hsu, K. M. Hsu, M. K. Leong and I. J. B. Lin, *Dalton Trans.*, 2008, 1924–1931.
19 S. Myllynen and M. Wasberg, *Electrochem. Commun.*, 2009, **11**, 1453–1456.
20 M. Mitsumi, H. Ueda, K. Furukawa, Y. Ozawa, K. Toriumi and M. Kurmoo, *J. Am. Chem. Soc.*, 2008, **130**, 14102–14104.
21 A. Guijarro, O. Castillo, A. Calzolari, P. J. S. Miguel, C. J. Gómez-García, R. di Felice and F. Zamora, *Inorg. Chem.*, 2008, **47**, 9736–9738.
22 M. Mitsumi, H. Goto, S. Umebayashi, Y. Ozawa, M. Kobayashi, T. Yokoyama, H. Tanaka, S.-i. Kuroda and K. Toriumi, *Angew. Chem., Int. Ed.*, 2005, **44**, 4164–4168.
23 T. Seki, K. Sakurada, M. Muromoto, S. Seki and H. Ito, *Chem. – Eur. J.*, 2016, **22**, 1968–1978.
24 R. N. McDougald, B. Chilukuri, H. Jia, M. R. Perez, H. Rabaâ, X. Wang, V. N. Nesterov, T. R. Cundari, B. E. Gnade and M. A. Omary, *Inorg. Chem.*, 2014, **53**, 7485–7499.
25 V. P. Georgiev, P. J. Mohan, D. DeBrincat and J. E. McGrady, *Coord. Chem. Rev.*, 2013, **257**, 290–298.
26 R. H. Ismayilov, W.-Z. Wang, G.-H. Lee, C.-Y. Yeh, S.-A. Hua, Y. Song, M.-M. Rohmer, M. Bénard and S.-M. Peng, *Angew. Chem., Int. Ed.*, 2011, **50**, 2045–2048.
27 S. Bestgen, M. T. Gamer, S. Lebedkin, M. M. Kappes and P. W. Roesky, *Chem. – Eur. J.*, 2015, **21**, 601–614.
28 C. Kaub, S. Lebedkin, S. Bestgen, R. Köppe, M. M. Kappes and P. W. Roesky, *Chem. Commun.*, 2017, **53**, 9578–9581.
29 S. Schäfer, M. T. Gamer, S. Lebedkin, F. Weigend, M. M. Kappes and P. W. Roesky, *Chem. – Eur. J.*, 2017, **23**, 12198–12209.
30 T. P. Seifert, N. D. Knoefel, T. J. Feuerstein, K. Reiter, S. Lebedkin, M. T. Gamer, A. C. Boukis, F. Weigend, M. M. Kappes and P. W. Roesky, *Chem. – Eur. J.*, 2019, **25**, 3799–3808.
31 N. D. Knöfel, C. Schoo, T. P. Seifert and P. W. Roesky, *Dalton Trans.*, 2020, **49**, 1513–1521.

32 G. S. M. Tong, S. C. F. Kui, H.-Y. Chao, N. Zhu and C.-M. Che, *Chem. – Eur. J.*, 2009, **15**, 10777–10789.
33 D. Li, C.-M. Che, S.-M. Peng, S.-T. Liu, Z.-Y. Zhou and T. C. W. Mak, *J. Chem. Soc., Dalton Trans.*, 1993, 189–194.
34 T. Tanase, R. Otaki, T. Nishida, H. Takenaka, Y. Takemura, B. Kure, T. Nakajima, Y. Kitagawa and T. Tsubomura, *Chem. – Eur. J.*, 2014, **20**, 1577–1596.
35 L. H. Doerrer, *Dalton Trans.*, 2010, **39**, 3543–3553.
36 A. Aliprandi, D. Genovese, M. Mauro and L. D. Cola, *Chem. Lett.*, 2015, **44**, 1152–1169.
37 H. B. Gray, S. Záliš and A. Vlček, *Coord. Chem. Rev.*, 2017, **345**, 297–317.
38 M. J. Katz, K. Sakai and D. B. Leznoff, *Chem. Soc. Rev.*, 2008, **37**, 1884–1895.
39 S. Sculfort and P. Braunstein, *Chem. Soc. Rev.*, 2011, **40**, 2741–2760.
40 M. Stollenz, *Chem. – Eur. J.*, 2019, **25**, 4274–4298.
41 S.-A. Hua, M.-C. Cheng, C.-h. Chen and S.-M. Peng, *Eur. J. Inorg. Chem.*, 2015, **2015**, 2510–2523.
42 J. K. Bera and K. R. Dunbar, *Angew. Chem., Int. Ed.*, 2002, **41**, 4453–4457.
43 B. Lippert, *Coord. Chem. Rev.*, 1999, **182**, 263–295.
44 J. A. Chipman and J. F. Berry, *Chem. Rev.*, 2020, **120**, 2409–2447.
45 G. Aromí, *Comments Inorg. Chem.*, 2011, **32**, 163–194.
46 R. D. Riley, D. A. Dickie, M. A. Land, R. A. Kemp, C. L. B. Macdonald, U. Werner-Zwanziger, K. N. Robertson and J. A. C. Clyburne, *Chem. – Eur. J.*, 2020, **26**, 7711–7719.
47 V. W.-W. Yam, V. K.-M. Au and S. Y.-L. Leung, *Chem. Rev.*, 2015, **115**, 7589–7728.
48 V. W.-W. Yam, K. M.-C. Wong and N. Zhu, *J. Am. Chem. Soc.*, 2002, **124**, 6506–6507.
49 V. G. Andrianov, Y. T. Struchkov and E. R. Rossinskaja, *J. Chem. Soc., Chem. Commun.*, 1973, 338–339.
50 P. G. Jones, *Gold Bull.*, 1981, **14**, 102–118.
51 M. Melnínk and R. V. Parish, *Coord. Chem. Rev.*, 1986, **70**, 157–257.
52 J. J. Rehr, E. Zaremba and W. Kohn, *Phys. Rev. B: Condens. Matter Mater. Phys.*, 1975, **12**, 2062–2066.
53 P. Pyykkö and Y. Zhao, *Angew. Chem., Int. Ed. Engl.*, 1991, **30**, 604–605.
54 P. Pyykkö and F. Mendizabal, *Chem. – Eur. J.*, 1997, **3**, 1458–1465.
55 N. Runeberg, M. Schütz and H.-J. Werner, *J. Chem. Phys.*, 1999, **110**, 7210–7215.
56 P. Pyykkö, *Angew. Chem., Int. Ed.*, 2004, **43**, 4412–4456.
57 P. Schwerdtfeger, A. E. Bruce and M. R. M. Bruce, *J. Am. Chem. Soc.*, 1998, **120**, 6587–6597.
58 P. Pyykkö, *Chem. Soc. Rev.*, 2008, **37**, 1967–1997.
59 P. Pyykkö, *Inorg. Chim. Acta*, 2005, **358**, 4113–4130.
60 G. J. Hutchings, M. Brust and H. Schmidbaur, *Chem. Soc. Rev.*, 2008, **37**, 1759–1765.
61 H. Schmidbaur, *Gold Bull.*, 2000, **33**, 3–10.
62 M. B. Brands, J. Nitsch and C. F. Guerra, *Inorg. Chem.*, 2018, **57**, 2603–2608.
63 E. Andris, P. C. Andrikopoulos, J. Schulz, J. Turek, A. Růžička, J. Roithová and L. Rulíšek, *J. Am. Chem. Soc.*, 2018, **140**, 2316–2325.
64 H. Schmidbaur, *Gold Bull.*, 1990, **23**, 11–21.
65 F. Scherbaum, A. Grohmann, G. Müller and H. Schmidbaur, *Angew. Chem., Int. Ed. Engl.*, 1989, **28**, 463–465.
66 S. Alvarez, *Dalton Trans.*, 2013, **42**, 8617–8636.
67 H. Schmidbaur and A. Schier, *Chem. Soc. Rev.*, 2008, **37**, 1931–1951.
68 H. Schmidbaur and A. Schier, *Chem. Soc. Rev.*, 2012, **41**, 370–412.
69 M. A. Rawashdeh-Omary, M. A. Omary and H. H. Patterson, *J. Am. Chem. Soc.*, 2000, **122**, 10371–10380.
70 J. C. Y. Lin, S. S. Tang, C. S. Vasam, W. C. You, T. W. Ho, C. H. Huang, B. J. Sun, C. Y. Huang, C. S. Lee, W. S. Hwang, A. H. H. Chang and I. J. B. Lin, *Inorg. Chem.*, 2008, **47**, 2543–2551.
71 F. Balzano, A. Cuzzola, P. Diversi, F. Ghiotto and G. Uccello-Barretta, *Eur. J. Inorg. Chem.*, 2007, **2007**, 5556–5562.
72 Z. Lei, J.-Y. Zhang, Z.-J. Guan and Q.-M. Wang, *Chem. Commun.*, 2017, **53**, 10902–10905.
73 H. de la Riva, A. Pintado-Alba, M. Nieuwenhuyzen, C. Hardacre and M. C. Lagunas, *Chem. Commun.*, 2005, 4970–4972.
74 P. K. Mehrotra and R. Hoffmann, *Inorg. Chem.*, 1978, **17**, 2187–2189.
75 M. Jansen, *Angew. Chem., Int. Ed. Engl.*, 1987, **26**, 1098–1110.
76 S. Sculfort, P. Croizat, A. Messaoudi, M. Bénard, M.-M. Rohmer, R. Welter and P. Braunstein, *Angew. Chem., Int. Ed.*, 2009, **48**, 9663–9667.
77 E. J. Fernández, P. G. Jones, A. Laguna, J. M. López-de-Luzuriaga, M. Monge, J. Pérez and M. E. Olmos, *Inorg. Chem.*, 2002, **41**, 1056–1063.
78 E. M. Gussenhoven, M. M. Olmstead, J. C. Fettinger and A. L. Balch, *Inorg. Chem.*, 2008, **47**, 4570–4578.
79 L. H. Doerrer, *Comments Inorg. Chem.*, 2008, **29**, 93–127.
80 M. Kim, T. J. Taylor and F. P. Gabbaï, *J. Am. Chem. Soc.*, 2008, **130**, 6332–6333.
81 N. Masciocchi, M. Moret, P. Cairati, F. Ragaini and A. Sironi, *J. Chem. Soc., Dalton Trans.*, 1993, 471–475.
82 H. Schmidbaur, S. Cronje, B. Djordjevic and O. Schuster, *Chem. Phys.*, 2005, **311**, 151–161.
83 P. Pyykkö, *Annu. Rev. Phys. Chem.*, 2012, **63**, 45–64.
84 X. He and V. W.-W. Yam, *Coord. Chem. Rev.*, 2011, **255**, 2111–2123.
85 V. W.-W. Yam and E. C.-C. Cheng, *Chem. Soc. Rev.*, 2008, **37**, 1806–1813.
86 V. W.-W. Yam and K. K.-W. Lo, *Chem. Soc. Rev.*, 1999, **28**, 323–334.
87 J. C. Koziar and D. O. Cowan, *Acc. Chem. Res.*, 1978, **11**, 334–341.
88 C.-K. Li, X.-X. Lu, K. M.-C. Wong, C.-L. Chan, N. Zhu and V. W.-W. Yam, *Inorg. Chem.*, 2004, **43**, 7421–7430.

89 S. K. Chastain and W. R. Mason, *Inorg. Chem.*, 1982, **21**, 3717–3721.
90 M. M. Savas and W. R. Mason, *Inorg. Chem.*, 1987, **26**, 301–307.
91 A. Vogler and H. Kunkely, *Coord. Chem. Rev.*, 2001, **219–221**, 489–507.
92 V. W.-W. Yam and E. C.-C. Cheng, in *Photochemistry and Photophysics of Coordination Compounds II*, ed. V. Balzani and S. Campagna, Springer Berlin Heidelberg, Berlin, Heidelberg, 2007, pp. 269–309.
93 V. W.-W. Yam, T.-F. Lai and C.-M. Che, *J. Chem. Soc., Dalton Trans.*, 1990, 3747–3752.
94 J. C. Vickery, M. M. Olmstead, E. Y. Fung and A. L. Balch, *Angew. Chem., Int. Ed. Engl.*, 1997, **36**, 1179–1181.
95 M. Jin, T. Seki and H. Ito, *J. Am. Chem. Soc.*, 2017, **139**, 7452–7455.
96 A. L. Balch, *Angew. Chem., Int. Ed.*, 2009, **48**, 2641–2644.
97 K. M. Anderson, A. E. Goeta and J. W. Steed, *Inorg. Chem.*, 2007, **46**, 6444–6451.
98 H. Schmidbaur and H. G. Raubenheimer, *Angew. Chem., Int. Ed.*, 2020, **59**, 14748–14771.
99 A. Wuttke, M. Feldt and R. A. Mata, *J. Phys. Chem. A*, 2018, **122**, 6918–6925.
100 S. Ahrland, B. Noren and A. Oskarsson, *Inorg. Chem.*, 1985, **24**, 1330–1333.
101 M. Strey, C. Döring and P. G. Jones, *Z. Naturforsch., B: J. Chem. Sci.*, 2018, **73**, 125.
102 S. Ahrland, K. Dreisch, B. Norén and Å. Oskarsson, *Mater. Chem. Phys.*, 1993, **35**, 281–289.
103 W. Conzelmann, W. Hiller, J. Strähle and G. M. Sheldrick, *Z. Anorg. Allg. Chem.*, 1984, **512**, 169–176.
104 J. Vicente, M.-T. Chicote, M.-D. Abrisqueta, R. Guerrero and P. G. Jones, *Angew. Chem., Int. Ed. Engl.*, 1997, **36**, 1203–1205.
105 S.-L. Zheng, C. L. Nygren, M. Messerschmidt and P. Coppens, *Chem. Commun.*, 2006, 3711–3713.
106 M. Saitoh, A. L. Balch, J. Yuasa, K. Tada, M. Onoda, T. Nakashima and T. Kawai, *Langmuir*, 2011, **27**, 10947–10952.
107 J. E. Parks and A. L. Balch, *J. Organomet. Chem.*, 1974, **71**, 453–463.
108 R. L. White-Morris, M. M. Olmstead, F. Jiang, D. S. Tinti and A. L. Balch, *J. Am. Chem. Soc.*, 2002, **124**, 2327–2336.
109 D. Rios, D. M. Pham, J. C. Fettinger, M. M. Olmstead and A. L. Balch, *Inorg. Chem.*, 2008, **47**, 3442–3451.
110 D. Rios, M. M. Olmstead and A. L. Balch, *Dalton Trans.*, 2008, 4157–4164.
111 M. Saitoh, A. L. Balch, J. Yuasa and T. Kawai, *Inorg. Chem.*, 2010, **49**, 7129–7134.
112 T. A. Engesser, C. Friedmann, A. Martens, D. Kratzert, P. J. Malinowski and I. Krossing, *Chem. – Eur. J.*, 2016, **22**, 15085–15094.
113 I. Krossing and I. Raabe, *Angew. Chem., Int. Ed.*, 2004, **43**, 2066–2090.
114 T. A. Engesser, M. R. Lichtenthaler, M. Schleep and I. Krossing, *Chem. Soc. Rev.*, 2016, **45**, 789–899.
115 L. M. C. Luong, M. A. Malwitz, V. Moshayedi, M. M. Olmstead and A. L. Balch, *J. Am. Chem. Soc.*, 2020, **142**, 5689–5701.
116 R. L. White-Morris, M. M. Olmstead and A. L. Balch, *J. Am. Chem. Soc.*, 2003, **125**, 1033–1040.
117 M. A. Malwitz, S. H. Lim, R. L. White-Morris, D. M. Pham, M. M. Olmstead and A. L. Balch, *J. Am. Chem. Soc.*, 2012, **134**, 10885–10893.
118 T. H. Kim, Y. W. Shin, J. H. Jung, J. S. Kim and J. Kim, *Angew. Chem., Int. Ed.*, 2008, **47**, 685–688.
119 R. Li, F.-F. Xu, Z.-L. Gong and Y.-W. Zhong, *Inorg. Chem. Front.*, 2020, DOI: 10.1039/D0QI00779J.
120 R. Y. Liau, H. Ehlich, A. Schier and H. Schmidbaur, *Z. Naturforsch., B: J. Chem. Sci.*, 2002, **57b**, 1085–1089.
121 Z. Tang, A. P. Litvinchuk, H.-G. Lee and A. M. Guloy, *Inorg. Chem.*, 1998, **37**, 4752–4753.
122 N. L. Coker, J. A. Krause Bauer and R. C. Elder, *J. Am. Chem. Soc.*, 2004, **126**, 12–13.
123 N. L. Coker, C. E. Bedel, J. A. Krause and R. C. Elder, *Acta Crystallogr., Sect. E: Struct. Rep. Online*, 2006, **62**, m319–m321.
124 Z. Assefa, B. G. McBurnett, R. J. Staples, J. P. Fackler, B. Assmann, K. Angermaier and H. Schmidbaur, *Inorg. Chem.*, 1995, **34**, 75–83.
125 N. Aoyagi, Y. Shinha, A. Ikeda-Ohno, Y. Haga, K. Shimojo, N. R. Brooks, A. Izuoka, H. Naganawa, T. Kimura and K. Binnemans, *Cryst. Growth Des.*, 2015, **15**, 1422–1429.
126 M. I. Jeffrey and P. L. Breuer, *Miner. Eng.*, 2000, **13**, 1097–1106.
127 R. Y. Wan and J. D. Miller, *JOM*, 1986, **38**, 35–40.
128 T. J. Boggon and L. Shapiro, *Structure*, 2000, **8**, R143–R149.
129 D. M. Pham, D. Rios, M. M. Olmstead and A. L. Balch, *Inorg. Chim. Acta*, 2005, **358**, 4261–4269.
130 A. D. Nicholas, R. M. Bullard, R. D. Pike and H. H. Patterson, *Eur. J. Inorg. Chem.*, 2019, **2019**, 956–962.
131 M. Stender, M. M. Olmstead, A. L. Balch, D. Rios and S. Attar, *Dalton Trans.*, 2003, 4282–4287.
132 D. B. Leznoff and J. Lefebvre, *Gold Bull.*, 2005, **38**, 47–54.
133 W. Han, L. Yi, Z.-Q. Liu, W. Gu, S.-P. Yan, P. Cheng, D.-Z. Liao and Z.-H. Jiang, *Eur. J. Inorg. Chem.*, 2004, **2004**, 2130–2136.
134 J. R. Thompson, J. S. Ovens, V. E. Williams and D. B. Leznoff, *Chem. – Eur. J.*, 2013, **19**, 16572–16578.
135 J. Qu, W. Gu and X. Liu, *J. Coord. Chem.*, 2008, **61**, 618–626.
136 F. Baril-Robert, X. Li, M. J. Katz, A. R. Geisheimer, D. B. Leznoff and H. Patterson, *Inorg. Chem.*, 2011, **50**, 231–237.
137 J. S. Ovens and D. B. Leznoff, *Dalton Trans.*, 2011, **40**, 4140–4146.
138 D. B. Leznoff, B.-Y. Xue, B. O. Patrick, V. Sanchez and R. C. Thompson, *Chem. Commun.*, 2001, 259–260.
139 D. B. Leznoff, B.-Y. Xue, R. J. Batchelor, F. W. B. Einstein and B. O. Patrick, *Inorg. Chem.*, 2001, **40**, 6026–6034.
140 H. Zhang, J. Cai, X.-L. Feng, T. Li, X.-Y. Li and L.-N. Ji, *Inorg. Chem. Commun.*, 2002, **5**, 637–641.

141 A. Karadağ, A. Aydın, S. Dede, Ş. Tekin, Y. Yanar, B. H. Çadırcı, M. S. Soylu and Ö. Andaç, *New J. Chem.*, 2015, **39**, 8136–8152.
142 J. Suárez-Varela, H. Sakiyama, J. Cano and E. Colacio, *Dalton Trans.*, 2007, 249–256.
143 M.-C. Brandys and R. J. Puddephatt, *Chem. Commun.*, 2001, 1280–1281.
144 G.-F. Xu, Z.-Q. Liu, H.-B. Zhou, Y. Guo and D.-Z. Liao, *Aust. J. Chem.*, 2006, **59**, 640–646.
145 Y. Guo, Z.-Q. Liu, B. Zhao, Y.-H. Feng, G.-F. Xu, S.-P. Yan, P. Cheng, Q.-L. Wang and D.-Z. Liao, *CrystEngComm*, 2009, **11**, 61–66.
146 J. C. Ahern, R. J. Roberts, P. Follansbee, J. McLaughlin, D. B. Leznoff and H. H. Patterson, *Inorg. Chem.*, 2014, **53**, 7571–7579.
147 R. J. Roberts, J. C. Ahern, H. H. Patterson and D. B. Leznoff, *Eur. J. Inorg. Chem.*, 2016, **2016**, 2082–2087.
148 R. B. Arthur, A. D. Nicholas, R. J. Roberts, Z. Assefa, D. B. Leznoff and H. H. Patterson, *Gold Bull.*, 2018, **51**, 1–10.
149 M. L. Brown, J. S. Ovens and D. B. Leznoff, *Dalton Trans.*, 2017, **46**, 7169–7180.
150 Q. Liu, M. Xie, X. Chang, Q. Gao, Y. Chen and W. Lu, *Chem. Commun.*, 2018, **54**, 12844–12847.
151 Y. Chen, G. Cheng, K. Li, D. P. Shelar, W. Lu and C.-M. Che, *Chem. Sci.*, 2014, **5**, 1348–1353.
152 W. C. Kaska, H. A. Mayer, M. R. J. Elsegood, P. N. Horton, M. B. Hursthouse, C. Redshaw and S. M. Humphrey, *Acta Crystallogr., Sect. E: Struct. Rep. Online*, 2004, **60**, m563–m565.
153 G. A. Koutsantonis, G. I. Jenkins, P. A. Schauer, B. Szczepaniak, B. W. Skelton, C. Tan and A. H. White, *Organometallics*, 2009, **28**, 2195–2205.
154 A. Bauer, W. Schneider and H. Schmidbaur, *Inorg. Chem.*, 1997, **36**, 2225–2226.
155 H. Ehlich, A. Schier and H. Schmidbaur, *Z. Naturforsch., B: J. Chem. Sci.*, 2002, **57**, 890.
156 M. Böge and J. Heck, *Chem. – Eur. J.*, 2016, **22**, 6787–6792.
157 N. Mirzadeh, D. W. Drumm, J. Wagler, S. P. Russo and S. Bhargava, *Dalton Trans.*, 2013, **42**, 12883–12890.
158 J. D. E. T. Wilton-Ely, H. Ehlich, A. Schier and H. Schmidbaur, *Helv. Chim. Acta*, 2001, **84**, 3216–3232.
159 F. Mohr, E. Cerrada and M. Laguna, *Organometallics*, 2006, **25**, 644–648.
160 M.-E. Núñez Gaytán, S. Bernès, E. Rodríguez de San Miguel and J. de Gyves, *Acta Crystallogr., Sect. C: Cryst. Struct. Commun.*, 2004, **60**, m414–m417.
161 U. Siemeling, D. Rother, C. Bruhn, H. Fink, T. Weidner, F. Träger, A. Rothenberger, D. Fenske, A. Priebe, J. Maurer and R. Winter, *J. Am. Chem. Soc.*, 2005, **127**, 1102–1103.
162 D. Parker, P. S. Roy, G. Ferguson and M. M. Hunt, *Inorg. Chim. Acta*, 1989, **155**, 227–230.
163 M. Arita, K. Naka, Y. Morisaki and Y. Chujo, *Heteroat. Chem.*, 2012, **23**, 16–26.
164 M. O. Awaleh, F. Baril-Robert, C. Reber, A. Badia and F. Brisse, *Inorg. Chem.*, 2008, **47**, 2964–2974.
165 S. Ahrland, B. Aurivillius, K. Dreisch, B. Norén and Å. Oskarsson, *Acta Chem. Scand.*, 1992, **46**, 262–265.
166 A. J. Moro, B. Rome, E. Aguiló, J. Arcau, R. Puttreddy, K. Rissanen, J. C. Lima and L. Rodríguez, *Org. Biomol. Chem.*, 2015, **13**, 2026–2033.
167 S. S. Y. Chui, M. F. Y. Ng and C.-M. Che, *Chem. – Eur. J.*, 2005, **11**, 1739–1749.
168 X. Lu, M. S. Yavuz, H.-Y. Tuan, B. A. Korgel and Y. Xia, *J. Am. Chem. Soc.*, 2008, **130**, 8900–8901.
169 H. Imoto, S. Nishiyama, T. Yumura, S. Watase, K. Matsukawa and K. Naka, *Dalton Trans.*, 2017, **46**, 8077–8082.
170 R. L. White-Morris, M. Stender, D. S. Tinti, A. L. Balch, D. Rios and S. Attar, *Inorg. Chem.*, 2003, **42**, 3237–3244.
171 R. L. White-Morris, M. M. Olmstead, A. L. Balch, O. Elbjeirami and M. A. Omary, *Inorg. Chem.*, 2003, **42**, 6741–6748.
172 H. Ecken, M. M. Olmstead, B. C. Noll, S. Attar, B. Schlyer and A. L. Balch, *J. Chem. Soc., Dalton Trans.*, 1998, 3715–3720.
173 D. V. Toronto, B. Weissbart, D. S. Tinti and A. L. Balch, *Inorg. Chem.*, 1996, **35**, 2484–2489.
174 B. Weissbart, D. V. Toronto, A. L. Balch and D. S. Tinti, *Inorg. Chem.*, 1996, **35**, 2490–2496.
175 P. Pyykkö, J. Li and N. Runeberg, *Chem. Phys. Lett.*, 1994, **218**, 133–138.
176 J. Braese, A. Schinabeck, M. Bodensteiner, H. Yersin, A. Y. Timoshkin and M. Scheer, *Chem. – Eur. J.*, 2018, **24**, 10073–10077.
177 S. Nath, S. K. Ghosh, S. Kundu, S. Praharaj, S. Panigrahi and T. Pal, *J. Nanopart. Res.*, 2006, **8**, 111–116.
178 F. Guyon, A. Hameau, A. Khatyr, M. Knorr, H. Amrouche, D. Fortin, P. D. Harvey, C. Strohmann, A. L. Ndiaye, V. Huch, M. Veith and N. Avarvari, *Inorg. Chem.*, 2008, **47**, 7483–7492.
179 P. J. Sadler, *J. Rheumatol., Suppl.*, 1982, **8**, 71–78.
180 C. Lavenn, N. Guillou, M. Monge, D. Podbevšek, G. Ledoux, A. Fateeva and A. Demessence, *Chem. Commun.*, 2016, **52**, 9063–9066.
181 R. G. Pearson, *J. Chem. Educ.*, 1968, **45**, 581.
182 R. G. Pearson, *J. Chem. Educ.*, 1968, **45**, 643.
183 D. Datta, *Inorg. Chem.*, 1992, **31**, 2797–2800.
184 R. G. Pearson, *Inorg. Chim. Acta*, 1995, **240**, 93–98.
185 T. A. Rodina, E. V. Korneeva, O. N. Antzutkin and A. V. Ivanov, *Spectrochim. Acta, Part A*, 2015, **149**, 881–888.
186 Y.-A. Lee, J. E. McGarrah, R. J. Lachicotte and R. Eisenberg, *J. Am. Chem. Soc.*, 2002, **124**, 10662–10663.
187 W. E. van Zyl, J. M. López-de-Luzuriaga, A. A. Mohamed, R. J. Staples and J. P. Fackler, *Inorg. Chem.*, 2002, **41**, 4579–4589.
188 E. V. Korneeva, T. A. Rodina, A. V. Ivanov, A. V. Gerasimenko and A. C. Larsson, *Russ. J. Coord. Chem.*, 2014, **40**, 748–756.
189 S. L. Lawton, W. J. Rohrbaugh and G. T. Kokotailo, *Inorg. Chem.*, 1972, **11**, 2227–2233.
190 J. Grote, B. Neumann, H.-G. Stammler and N. W. Mitzel, *Dalton Trans.*, 2018, **47**, 4701–4706.

191 M. L. Gallego, A. Guijarro, O. Castillo, T. Parella, R. Mas-Balleste and F. Zamora, *CrystEngComm*, 2010, **12**, 2332–2334.
192 H.-J. You, C.-S. Fang, J.-L. Lin, S.-S. Sun and C. W. Liu, *Inorg. Chem.*, 2010, **49**, 7641–7643.
193 C. Latouche, Y.-C. Lee, J.-H. Liao, E. Furet, J.-Y. Saillard, C. W. Liu and A. Boucekkine, *Inorg. Chem.*, 2012, **51**, 11851–11859.
194 R. J. Roberts, D. Le and D. B. Leznoff, *Chem. Commun.*, 2015, **51**, 14299–14302.
195 M.-R. Azani, O. Castillo, M. L. Gallego, T. Parella, G. Aullón, O. Crespo, A. Laguna, S. Alvarez, R. Mas-Ballesté and F. Zamora, *Chem. – Eur. J.*, 2012, **18**, 9965–9976.
196 S. Naeem, S. A. Serapian, A. Toscani, A. J. P. White, G. Hogarth and J. D. E. T. Wilton-Ely, *Inorg. Chem.*, 2014, **53**, 2404–2416.
197 S. S. Tang, C.-P. Chang, I. J. B. Lin, L.-S. Liou and J.-C. Wang, *Inorg. Chem.*, 1997, **36**, 2294–2300.
198 P. Bishop, P. Marsh, A. K. Brisdon, B. J. Brisdon and M. F. Mahon, *J. Chem. Soc., Dalton Trans.*, 1998, 675–682.
199 A. C. Lane, C. L. Barnes, M. V. Vollmer and J. R. Walensky, *Inorganics*, 2014, **2**, 540–551.
200 D. Paliwoda, P. Wawrzyniak and A. Katrusiak, *J. Phys. Chem. Lett.*, 2014, **5**, 2182–2188.
201 B.-C. Tzeng and A. Chao, *Chem. – Eur. J.*, 2015, **21**, 2083–2089.
202 T. Seki, K. Ida, H. Sato, S. Aono, S. Sakaki and H. Ito, *Chem. – Eur. J.*, 2020, **26**, 735–744.
203 H. Ito, M. Muromoto, S. Kurenuma, S. Ishizaka, N. Kitamura, H. Sato and T. Seki, *Nat. Commun.*, 2013, **4**, 2009.
204 T. Seki, K. Sakurada and H. Ito, *Angew. Chem., Int. Ed.*, 2013, **52**, 12828–12832.
205 T. Seki, Y. Takamatsu and H. Ito, *J. Am. Chem. Soc.*, 2016, **138**, 6252–6260.
206 Y.-A. Lee and R. Eisenberg, *J. Am. Chem. Soc.*, 2003, **125**, 7778–7779.
207 A. Hayashi, M. M. Olmstead, S. Attar and A. L. Balch, *J. Am. Chem. Soc.*, 2002, **124**, 5791–5795.
208 L. D. Earl, J. K. Nagle and M. O. Wolf, *Inorg. Chem.*, 2014, **53**, 7106–7117.
209 R. L. White-Morris, M. M. Olmstead, S. Attar and A. L. Balch, *Inorg. Chem.*, 2005, **44**, 5021–5029.
210 J. C. Vickery and A. L. Balch, *Inorg. Chem.*, 1997, **36**, 5978–5983.
211 K. Winkler, M. Wysocka-Żołopa, K. Rećko, L. Dobrzyński, J. C. Vickery and A. L. Balch, *Inorg. Chem.*, 2009, **48**, 1551–1558.
212 J.-L. Brédas, D. Beljonne, V. Coropceanu and J. Cornil, *Chem. Rev.*, 2004, **104**, 4971–5004.
213 J.-L. Brédas, J. Cornil, D. Beljonne, D. A. dos Santos and Z. Shuai, *Acc. Chem. Res.*, 1999, **32**, 267–276.
214 S. T. Bromley, M. Mas-Torrent, P. Hadley and C. Rovira, *J. Am. Chem. Soc.*, 2004, **126**, 6544–6545.
215 M. C. R. Delgado, K. R. Pigg, D. A. da Silva Filho, N. E. Gruhn, Y. Sakamoto, T. Suzuki, R. M. Osuna, J. Casado, V. Hernández, J. T. L. Navarrete, N. G. Martinelli, J. Cornil, R. S. Sánchez-Carrera, V. Coropceanu and J.-L. Brédas, *J. Am. Chem. Soc.*, 2009, **131**, 1502–1512.
216 C.-H. Li, C.-H. Huang and M.-Y. Kuo, *Phys. Chem. Chem. Phys.*, 2011, **13**, 11148–11155.
217 R. A. Marcus, *Rev. Mod. Phys.*, 1993, **65**, 599–610.
218 L. Zhu, V. Coropceanu, Y. Yi, B. Chilukuri, T. R. Cundari and J.-L. Brédas, *J. Phys. Chem. Lett.*, 2013, **4**, 2186–2189.
219 D. Yao, Y. Wang, P. Li, K. Müller-Buschbaum and H. Li, *Opt. Mater.*, 2019, **96**, 109371.
220 T. Wehner, J. Heck, C. Feldmann and K. Müller-Buschbaum, *Chem. – Eur. J.*, 2019, **25**, 16630–16638.
221 M. Natali and S. Giordani, *Chem. Soc. Rev.*, 2012, **41**, 4010–4029.
222 M.-C. Tang, A. K.-W. Chan, M.-Y. Chan and V. W.-W. Yam, in *Photoluminescent Materials and Electroluminescent Devices*, ed. N. Armaroli and H. J. Bolink, Springer International Publishing, Cham, 2017, pp. 67–109.
223 C. Bizzarri, E. Spuling, D. M. Knoll, D. Volz and S. Bräse, *Coord. Chem. Rev.*, 2018, **373**, 49–82.
224 Z. Liu, J. Qiu, F. Wei, J. Wang, X. Liu, M. G. Helander, S. Rodney, Z. Wang, Z. Bian, Z. Lu, M. E. Thompson and C. Huang, *Chem. Mater.*, 2014, **26**, 2368–2373.
225 L. P. Ravaro, K. P. S. Zanoni and A. S. S. de Camargo, *Energy Rep.*, 2020, **6**, 37–45.
226 I. Omae, *Coord. Chem. Rev.*, 2016, **310**, 154–169.
227 R. Hamze, J. L. Peltier, D. Sylvinson, M. Jung, J. Cardenas, R. Haiges, M. Soleilhavoup, R. Jazzar, P. I. Djurovich, G. Bertrand and M. E. Thompson, *Science*, 2019, **363**, 601.
228 D. M. Adams, L. Brus, C. E. D. Chidsey, S. Creager, C. Creutz, C. R. Kagan, P. V. Kamat, M. Lieberman, S. Lindsay, R. A. Marcus, R. M. Metzger, M. E. Michel-Beyerle, J. R. Miller, M. D. Newton, D. R. Rolison, O. Sankey, K. S. Schanze, J. Yardley and X. Zhu, *J. Phys. Chem. B*, 2003, **107**, 6668–6697.